NASA CR-159290

NASA CONTRACTOR REPORT 159290

Evaluation of Aero Commander Sidewall Vibration and Interior Acoustic Data : Static Operations

A. G. PIERSOL
E. G. WILBY
J. F. WILBY

BOLT BERANEK AND NEWMAN INC.
CANOGA PARK, CA. 91303

NASA

National Aeronautics and
Space Administration

Langley Research Center
Hampton, Virginia 23665

Evaluation of Aero Commander Sidewall Vibration and Interior Acoustic Data : Static Operations

A. G. PIERSOL
E. G. WILBY
J. F. WILBY

NASA
National Aeronautics and
Space Administration

Langley Research Center
Hampton, Virginia 23665

N80-33392

ABSTRACT

This report is the third in a series covering the analyses of
acoustic and vibration data from ground tests performed on an
Aero Commander propeller-driven aircraft with an array of micro-
phones and accelerometers mounted on one side of the fuselage.
Analyses of acoustic data acquired during static and taxi opera-
tions are summarized in NASA CR-158919 and NASA CR-159124,
respectively. This document contains results for the vibration
measured at five locations on the fuselage structure during static
operations. The analysis was concerned with the magnitude of the
vibration and the relative phase between different locations, the
frequency response (inertance) functions between the exterior
pressure field and the vibration, and the coherent output power
functions at interior microphone locations based on sidewall
vibration. The results indicate that fuselage skin panels near
the plane of rotation of the propeller accept propeller noise
excitation more efficiently than they do exhaust noise. However
the measurements were not extensive enough to determine the rela-
tive noise transmission paths, nor were they sufficient to
provide analyses of the flexural wave propagation in the structure.
Coherent output power measurements could separate contribu-
tions from right and left hand propellers as they occurred at
slightly different frequencies, but the measurements could not
identify the relative roles played by different structural ele-
ments in transmitting sound. Measured inertance functions show
broadband-type characteristics without the resonance peaks pre-
dicted by a simplified analysis. A more detailed analysis might
provide better agreement.

TABLE OF CONTENTS

LIST OF FIGURES

LIST OF TABLES

EVALUATION OF AERO COMMANDER SIDEWALL VIBRATION
AND INTERIOR ACOUSTIC DATA: STATIC OPERATIONS

1.0   INTRODUCTION AND OBJECTIVES

A series of acoustic noise and vibration experiments have been
performed by personnel of the NASA Langley Research Center
involving a reciprocating engine-propeller driven Aero Commander
airplane instrumented with flush-mounted exterior microphones
as well as interior accelerometers on the starboard fuselage
sidewall, and additional microphones inside the fuselage. The
data from most of the microphones have already been analyzed and
evaluated [1,2] for both static and taxi operations. Of primary
interest here are the data from the sidewall accelerometers and
their relationships to the microphone data during static
operations. Specifically, the following analyses are of concern.

(a)   The magnitude of the vibration and acoustic pressures*
      due to all significant propeller blade passage tones at
      various locations on the fuselage and inside the cabin.

(b)   The frequency response (inertance) functions between
      the exterior acoustic pressures and vibration responses
      at selected locations on the fuselage for both propeller
      blade passage and exhaust noise excitations.

---

*The microphone outputs will be referred to throughout as
 acoustic pressure signals although the signals from the
 exterior microphone often represent fluctuating pressures of
 aerodynamic origin rather than acoustic excitations.

(c) The relative phase between spatially separated vibration responses as well as spatially separated acoustic pressures at selected locations for both propeller blade passage and exhaust noise excitations.

(d) The coherent output power functions at the interior microphone locations based upon individual sidewall vibration responses.

The first analysis is intended to provide background information. Analysis (b) is designed to identify the relative transmission of propeller versus exhaust noise through the fuselage sidewall near the plane of the propellers. The purpose of analysis (c) is to investigate the possibility of significant flexural wave propagation of propeller and/or exhaust noise excitations down the fuselage structure based upon calculated trace velocities. The last analysis involving coherent output powers is intended to help identify the relative contributions of propeller and exhaust noise to the interior sound levels via fuselage transmission in the plane of the propeller.

This report summarizes the procedures and results of the above-noted analyses and their evaluations. The analyses were performed by Bolt Beranek and Newman Inc. (BBN) for the NASA Langley Research Center (LRC) under Task Assignment No. 32 of Contract NAS1-14611. Additional studies of the sidewall dynamics of the Aero Commander test airplane have been performed by LRC personnel and the results are presented in Ref. [3].

2.0   DATA AND INSTRUMENTATION

The data were provided for analysis by LRC in the form of magnetic
tape recordings of acceleration and acoustic pressure signals on a
14-channel tape recorder. The data were Frequency Modulated with
a carrier frequency of 54 kHz on intermediate range providing
a recorded data frequency range of 0 to 10 kHz at 30 ips.

2.1   Summary of Data

The recorded data included five channels of acceleration signals
and six channels of pressure signals for nine specific static
test conditions, as summarized in Table 1. The locations of the

Table 1. Summary of Aero Commander Static Test Runs

Run Number	Operating Engines	Nominal Engine Speed (rpm)	Blade Passage Frequency (Hz)	
			Nominal	Measured
9	Both	2100	67.4	66.6
10*	Both	2400	77.0	77.4
11	Both	2400	77.0	76.4
12	Both	2600	83.4	81.9
12b	Both	2600	83.4	82.0
13	Port only	2100	67.4	67.3
14*	Stbd only	2100	67.4	67.2
14b	Stbd only	2100	67.4	66.8
15	Stbd only	1700	54.5	54.7

*Deleted from analysis due to saturated signal recordings.

accelerometers and microphones are detailed in Figure 1. The accelerometers were mounted directly on the interior structure of the fuselage. Microphones 11 and 12 were located inside the fuselage near the cockpit. The other four microphones were flush mounted in the fuselage sidewall to sense exterior pressures. For test runs 10 and 14, some of the data channels appear to have been saturated during recording. Hence, these two runs were deleted from the analysis, as indicated in Table 1.

2.2   Summary of Analysis Instrumentation

The data records were reproduced for analysis using a Hewlett Packard 3924B magnetic tape recorder with appropriate FM reproduce electronics. All analyses were performed using the appropriate function on a Spectral Dynamics Model SD360 Digital Signal Processor. Various post analysis evaluations were accomplished using programmable hand calculators.

TRANSDUCERS	ACCELEROMETERS ●					MICROPHONES ▲					
Location	A1	A2	A3	A4	A5	M2	M4	M5	M7	M11*	M12**
x (meters)	-0.03	-0.03	-0.08	-0.16+	0.27	-0.37	0	0	0.37	0	0
y (meters)	0.89	0.68	0.40	0.40+	0.93	0.55	0.83	0.55	0.55	0.83	1.02

*M11 is Inside Fuselage 0.25 m Left of M4

**M12 is Inside Fuselage on Aircraft Centerline

+Approximate Location
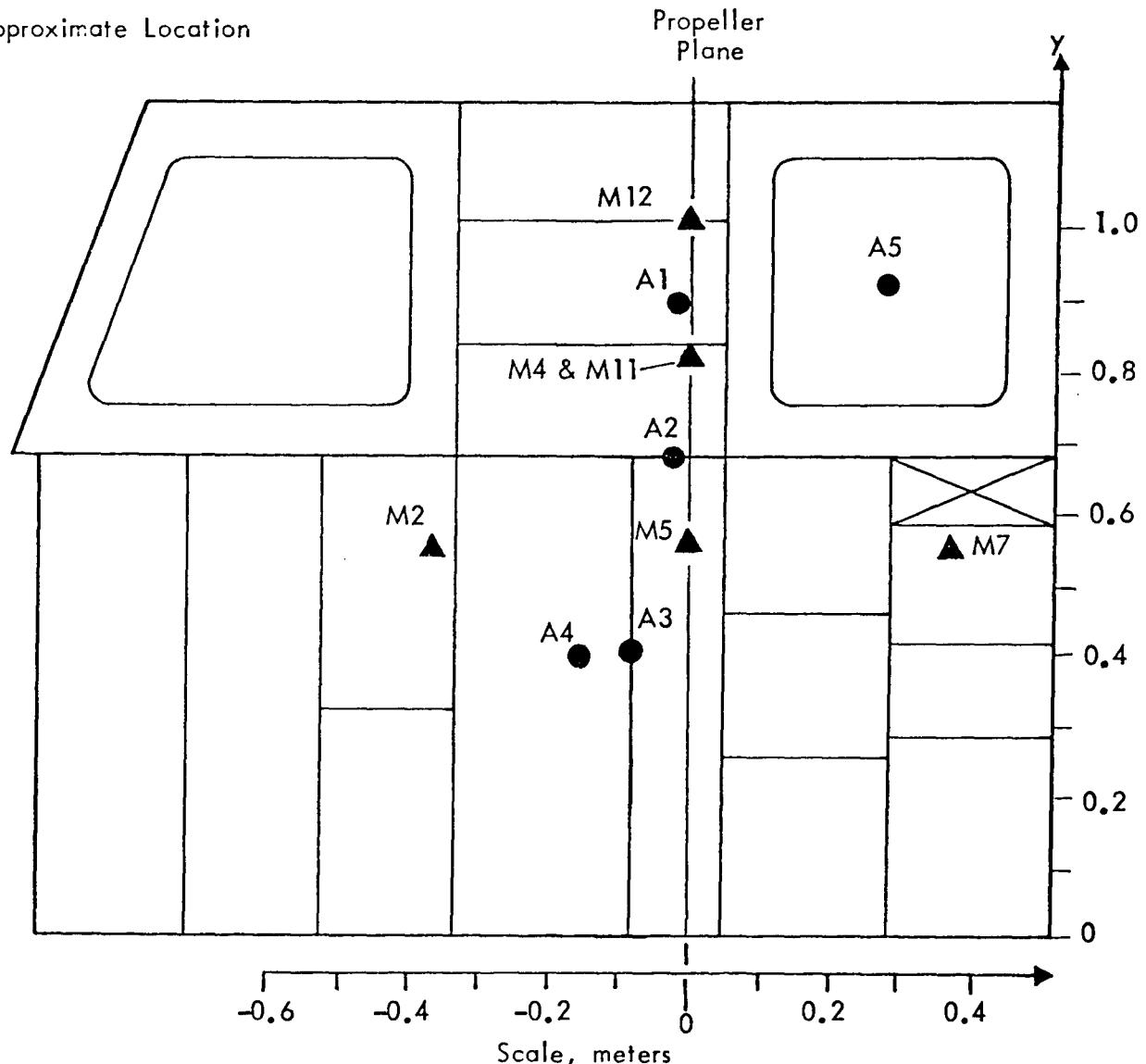
FIGURE 1.   LOCATION OF ACCELEROMETERS AND MICROPHONES FOR AERO COMMANDER STATIC TEST RUNS

3.   DATA ANALYSIS PROCEDURES

The required data analyses are broadly divided into four categories, as previously summarized in Section 1. To be consistent with earlier studies of similar data [1,2], all spectral analyses including coherence and phase computations were performed with a resolution bandwidth of B_e = 2 Hz. The referenced earlier studies indicated that a 2 Hz bandwidth constituted a good compromise between resolution power and the actual bandwidth of individual propeller blade passage tones.

3.1   Propeller Induced Vibration and Acoustic Levels

This analysis was performed on the SD360 using Function 3 (2048 point forward transform) with a Kaiser-Bessel time window. The frequency range for the analysis was 0 to 2 kHz (B_e = 2 Hz) which was adequate to cover at least the first 20 harmonics of the propeller blade passage excitation for all test conditions.

Calibration of the vibration data was accomplished by analyzing the vibration calibration signals on the tape (0.5 volts at 260 Hz) using exactly the same analyzer settings employed later for the actual vibration data analysis. The vibration data were then read out of the analyzer in dB referenced to the calibration signal, i.e., dB (ref: 0.5 volts). Finally, these data were converted to dB referenced to 1 g (9.8 m/s^2) using accelerometer sensitivity factors provided by LRC. The acoustic data were calibrated in a similar way using the recorded acoustic calibration signals (124 dB at 250 Hz). Based upon calibrations of individual components in the data acquisition system by LRC personnel, the frequency response function of the acquisition system was assumed to be acceptably flat.

Fourier spectra of the vibration data from all five accelerometers and the fluctuating pressure data from microphones 4, 5, 11 and 12 in Figure 1 were computed for all valid test runs in Table 1. The Fourier magnitudes of the data at the propeller blade passage frequencies through the 20th harmonic were read off and tabulated. The vibration data as well as the acoustic data from microphone 12 represent new information. However, similar data for microphones 4, 5 and 11 are available from the results of two previous Aero Commander experiments [1,2]. The analysis of these measurement locations was accomplished here to evaluate the repeatability of data from one experiment to the next. The data from microphones 2 and 7 also represented a duplication of prior measurements and, hence, were not analyzed.

3.2   Acoustic/Vibration Frequency Response Functions

The analysis here was performed on the SD360 using Function 6 (transfer function B/A) which calculates the frequency response function between two signal x(t) and y(t) using the relationship

$$H_{xy}(f) = G_{xy}(f)/G_{xx}(f) \tag{1}$$

where $G_{xy}(f)$ is the cross-spectrum between x(t) and y(t) and $G_{xx}(f)$ is the autospectrum of x(t). The analyzer employs a 1024 point block size for the Fourier transform computations needed to arrive at the auto and cross spectra. Hence, to achieve the desired B_e = 2 Hz resolution, the analysis was restricted to a frequency range of 0 to 1 kHz. The input and output for the frequency response calculations were x(t) = pressure excitation and y (t) = acceleration response, yielding what is often called an inertance function. The magnitude of the inertance function was calibrated in dB referenced to 1 g per

20 $\mu N/m^2$ so the addition of a pressure measurement in dB to $|H_{xy}(f)|$ in dB will directly yield the vibration response in dB referenced to 1 g. The calibration was accomplished by measuring the magnitudes of the individual pressure and acceleration signals at the first few propeller blade passage frequencies where the coherence between the two signals was almost unity. When the coherence function given by

$$\gamma_{xy}^2(f) = \frac{|G_{xy}(f)|^2}{G_{xx}(f)\ G_{yy}(f)} \tag{2}$$

is approximately unity, it follows from Eqs. (1) and (2) that

$$|H_{xy}(f)|^2 \simeq G_{yy}(f)/G_{xx}(f) \tag{3}$$

Hence, the calibration of $|H_{xy}(f)|^2$ in dB is given by dB $[G_{yy}(f)]$ – dB $[G_{xx}(f)]$ where the calibration of the input and output signals was accomplished as detailed in Section 3.1.

Seven pairs of pressure and acceleration measurements were selected for inertance magnitude analysis, as detailed in Table 2. The A1/M4 and A4/M7 pairs were analyzed for all valid test runs in Table 1. All other pairs were analyzed for the 2600 rpm condition (test run 12b) only. Inertance magnitude values were read off and tabulated at frequencies corresponding to the first ten propeller blade passage harmonics and the first 38 engine exhaust harmonics, as detailed in Appendix A. The values computed at propeller versus exhaust frequencies were separately identified so that direct comparisons could be made between the sidewall inertance functions for the propeller and exhaust excitations. Because of their relevance to possible random errors in frequency response function estimates [4], coherence function values defined by Eq. (2) were also calculated and used to assess whether an

inertance estimate was meaningful. Specifically, only those
inertance estimates with a coherence of greater than 0.1 or so
were recorded.

Table 2.   Microphone/Accelerometer Pairs For
           Inertance Calculations

Microphone Number (see Fig. 1)	Accelerometer Number (see Fig. 1)				
	A1	A2	A3	A4	A5
M4	x	x			x
M5			x		
M7			x	x	x

3.3 Phase Functions Between Spatially Separated Measurements

Phase angle calculations were accomplished on the SD360 using
Function 6, exactly as for the inertance calculations in Section 3.2.
The desired phase calculation is simply the phase factor of the
frequency response function $H_{xy}(f)$, which in turn is the phase
factor of the cross-spectrum $G_{xy}(f)$ [5].   Noting that $G_{xy}(f)$ is
a complex number

$$G_{xy}(f) = C_{xy}(f) - jQ_{xy}(f) \tag{4}$$

the phase is given by

$$\phi_{xy}(f) = \tan^{-1} \frac{Q_{xy}(f)}{C_{xy}(f)} \tag{5}$$

Since the phase between two signals is not related to their
magnitudes, no calibration was needed for the phase calculations.
However, possible phase errors in the data acquisition system
are of concern. Based upon system phase evaluations performed
by LRC personnel, it was assumed that data acquisition phase
errors were negligible.

The purpose of the phase measurements was to establish trace velocities for both acoustic and vibratory energy over and/or through the sidewall structure. It follows that measurements between both vertically and longitudinally spaced transducers were desired. Seven such pairs of transducers, including five accelerometer pairs and two microphone pairs were analyzed, as detailed in Table 3. Phase data were computed for all

Table 3. Microphone and Accelerometer Pairs
For Relative Phase Calculations

Transducer (see Fig. 1)	A1	A2	A3	A4	A5	M4	M5	M7
A1	--	x	x	x	x			
A3			--	x				
M5						x	--	x

valid test runs in Table 1 for accelerometer pairs A1/A4 and A3/A4. Phase data for all other pairs of transducers in Table 3 were calculated for the 2600 rpm operation (test run 12b) only.

As for the inertance function calculations in Section 3.2, phase values were read off and tabulated at frequencies corresponding to the first ten propeller blade passage harmonics and separately for the first 38 engine exhaust harmonics, as detailed in Appendix A. Again, phase values were recorded only when the coherence function per Eq. (2) was greater than 0.1.

3.4 Vibration/Acoustic Coherent Output Power Functions

This final analysis was also performed using Function 6 on the SD360. The calculation here was for the coherent output of an

interior microphone signal $y(t)$ based upon a sidewall accelera-
tion measurement $x(t)$ as follows.

$$G_{y:x}(f) = \gamma^2_{xy}(f)G_{yy}(f) \tag{6}$$

where $G_{yy}(f)$ is the autospectrum of $y(t)$ and $\gamma^2_{xy}(f)$ is the
coherence function between $x(t)$ and $y(t)$. Since the coherence
function is dimensionless, only the output microphone signal $y(t)$
required calibration. This calibration was accomplished using
the 124 dB calibration signal at 250 Hz on the tape, as discussed
previously in Section 3.1.

The analysis was performed using ten transducer pairs, namely,
interior microphones No. 11 and 12 with each of the five
accelerometers in Figure 1. The test runs analyzed included 9,
12b and 14 in Table 1. These runs cover operations with both
engines and the starboard engine only at 2100 rpm, and both
engines at 2600 rpm. Coherent output power and overall values
for microphones No. 11 and 12 were read off and tabulated at
frequencies corresponding to the first ten propeller blade
passage harmonics and the first 38 exhaust harmonics for the
2600 rpm operation with both engines (run 12b), as detailed in
Appendix A. The results at propeller blade passage frequencies
only were recorded for the 2100 rpm operation (runs 9 and 14).

4.   RESULTS AND DISCUSSIONS

The results of the various studies are now summarized with
appropriate discussions of the interpretations.

4.1   Propeller Induced Vibration and Acoustic Levels

The magnitude of the significant vibration and acoustic levels
at frequencies corresponding to the first 20 propeller blade
passage harmonics for all locations in Figure 1 and for all
valid test runs in Table 1 are detailed in Appendix B. The
overall values of the vibration and acoustic pressure levels
are summarized by engine rpm in Table 4. Also presented in
this table are the test run number, the operating engines and
the actual propeller blade passage frequency (bpf) in Hz.

The results for two of the test runs in Table 4, namely, 12
and 12b, represent nearly identical operating conditions with
both engines operating at a nominal speed of 2600 rpm. Note
that the overall vibration values for these runs agree to
within 10% and the acoustic levels agree to within 0.3 dB.
Referring to the detailed results for runs 12 and 12b in
Appendix B, the spectra of the data for these two runs are
also in reasonable agreement.

A better check on the reproducibility of test results is pro-
vided by the acoustic pressure measurements at locations M4,
M5, and M11. The propeller blade passage induced pressures at
the same three locations were measured independently during two
previous Aero Commander experiments, one involving static
operations only [1] and the other including static operations
at 2600 rpm prior to taxi runs [2]. The overall levels from

Table 4. Overall Values of Propeller Induced
Vibration and Acoustic Levels

Engine rpm	1700	2100			2400	2600	
Run Number*	15	9	13	14b	11	12	12b
Engines Operating	Stbd	Both	Port	Stbd	Both	Both	Both
Actual bpf (Hz)	54.7	66.6	67.3	66.8	76.4	81.9	82.0
Location**	Overall Vibration Value in g rms						
A1	4.4	4.1	0.13	3.9	7.7	15.5	14.0
A2	0.33	0.46	0.07	0.45	0.67	1.0	1.0
A3	0.24	0.45	0.06	0.43	0.83	1.3	1.3
A4	0.64	1.8	0.10	1.9	4.6	6.1	6.1
A5	1.4	2.4	0.26	2.3	6.2	8.5	7.9
Location**	Overall Pressure Level in dB (ref: $20\mu N/m^2$)						
M4	127.4	131.5	103.2	132.0	135.7	137.6	137.8
M5	123.4	128.1	100.6	128.1	131.9	133.9	133.6
M11	95.2	102.6	100.2	99.2	105.7	106.4	106.6
M12	101.7	107.2	101.3	107.1	106.5	106.6	106.8

* See Table 1

** See Figure 1

all three experiments measured during similar operations are
compared in Table 5. Note that the results agree to within 1 dB
at all locations and for all comparable operating conditions.

Table 5. Overall Propeller Induced Pressure
Levels From Three Similar Experiments

Microphone Number	Experiment	Overall Pressure Level in dB* (ref:20μN/m²)			
		1700 rpm Stbd only	2100 rpm Stbd only	2400 rpm both	2600 rpm both
M4	Current	127.4	132.0	135.7	137.7
	Ref. [1]	127.1	131.7	135.2	137.2
	Ref. [2]	**	**	**	137.6
M5	Current	123.4	128.1	131.9	133.8
	Ref. [1]	123.2	128.5	131.8	133.9
	Ref. [2]	**	**	**	134.8
M11	Current	95.2	99.2	105.7	106.5
	Ref. [1,2]	94.6	100.0	105.8	107.3
	Ref. [2]	**	**	**	107.5

*   Average value when the experiment involved two runs at same
    condition.
** No data acquired.

Now concerning the spectra of the data, plots of the Fourier
spectra for microphone 4, accelerometer 1, and microphone 11
during operation of both engines at 2600 rpm (test run 12b) are
shown in Figure 2. From Figure 1, these three locations are in
the same region. Microphone 4, which senses the exterior
pressures in the plane of the propeller, is only 0.14m from
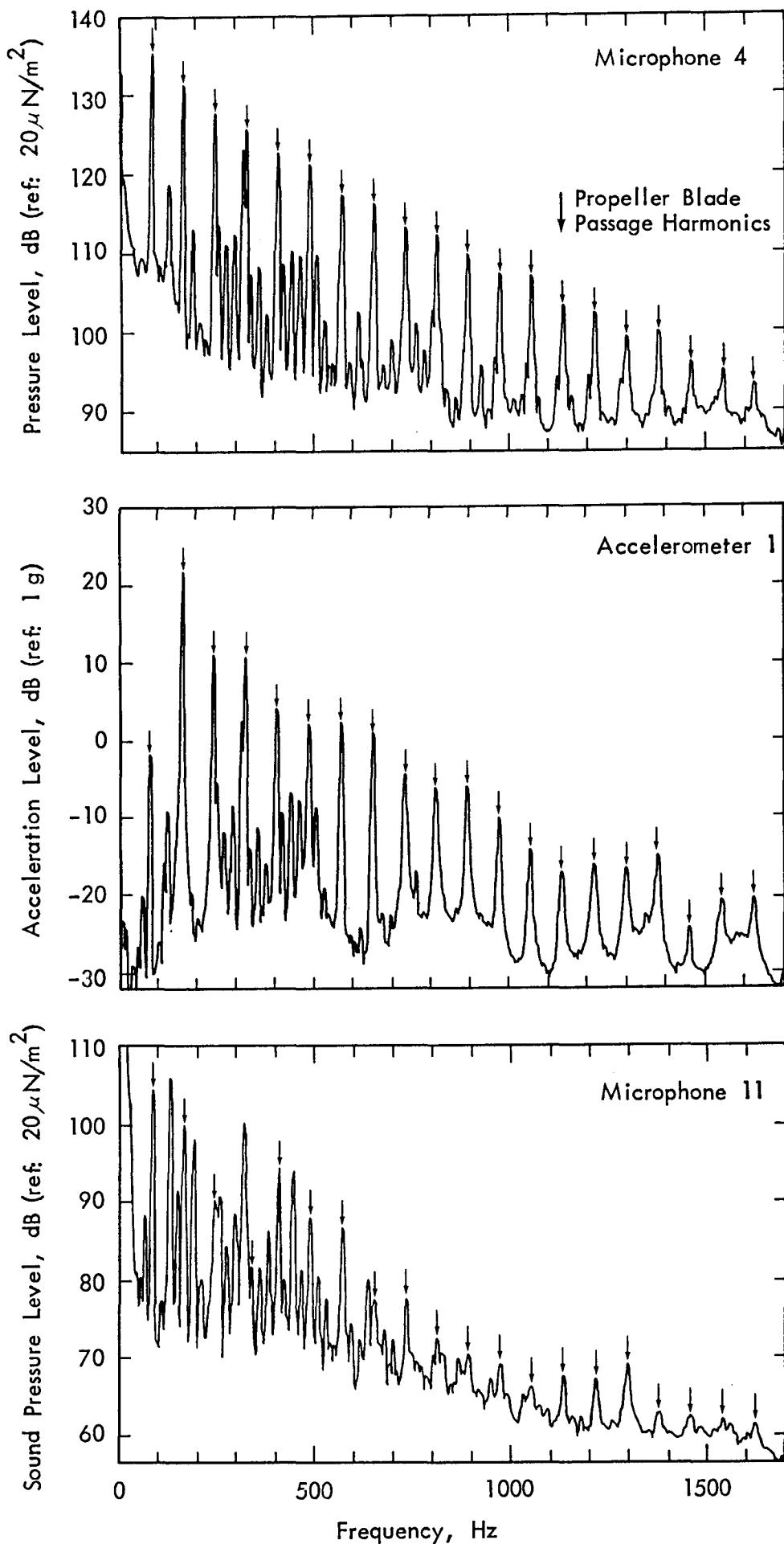
FIGURE 2. SPECTRA OF PRESSURE AND VIBRATION MEASUREMENTS NEAR PROPELLER PLANE FOR OPERATION AT 2600 rpm

accelerometer 1 mounted on a sidewall panel. Microphone 11, which senses acoustic noise inside the fuselage, is 0.25m inboard of microphone 4. These results, which are typical of all the data, reveal two interesting facts. First, although the propeller blade passage tones dominate the exterior pressure and acceleration data (M4 and A1), exhaust tones appear to control the interior acoustic noise. Second, the exhaust tones are somewhat more intense in the exterior pressure data than in the acceleration response. For example, the strong exhaust tone just before the fourth propeller harmonic is only about 3 dB below that propeller tone in the pressure data, but is a full 8 dB down from the same propeller tone in the acceleration data. These results indicate that the exhaust noise portions of the fuselage interior acoustic levels in the plane of the propeller do not transmit through the fuselage in this region, but instead must enter the fuselage through some other region (probably aft) and then propagate forward through the fuselage interior air space.

Another interesting aspect of the results in Figure 2 is that the propeller blade passage tones in the sidewall acceleration data (A1) fall with increasing frequency above 200 Hz at about the same rate as the propeller tones in the exterior pressure data (M4), as would be expected for a mass controlled vibration response. This is illustrated in Figure 3, which shows the ratio of acceleration A1 to pressure M4 for the 2600 rpm operation (average of test runs 12 and 12b). Note that the acceleration per unit pressure rises rapidly to a peak value at about 160 Hz, suggesting a stiffness controlled vibration response below this frequency. However, above 160 Hz, the curve oscillates about a constant value indicative of a mass
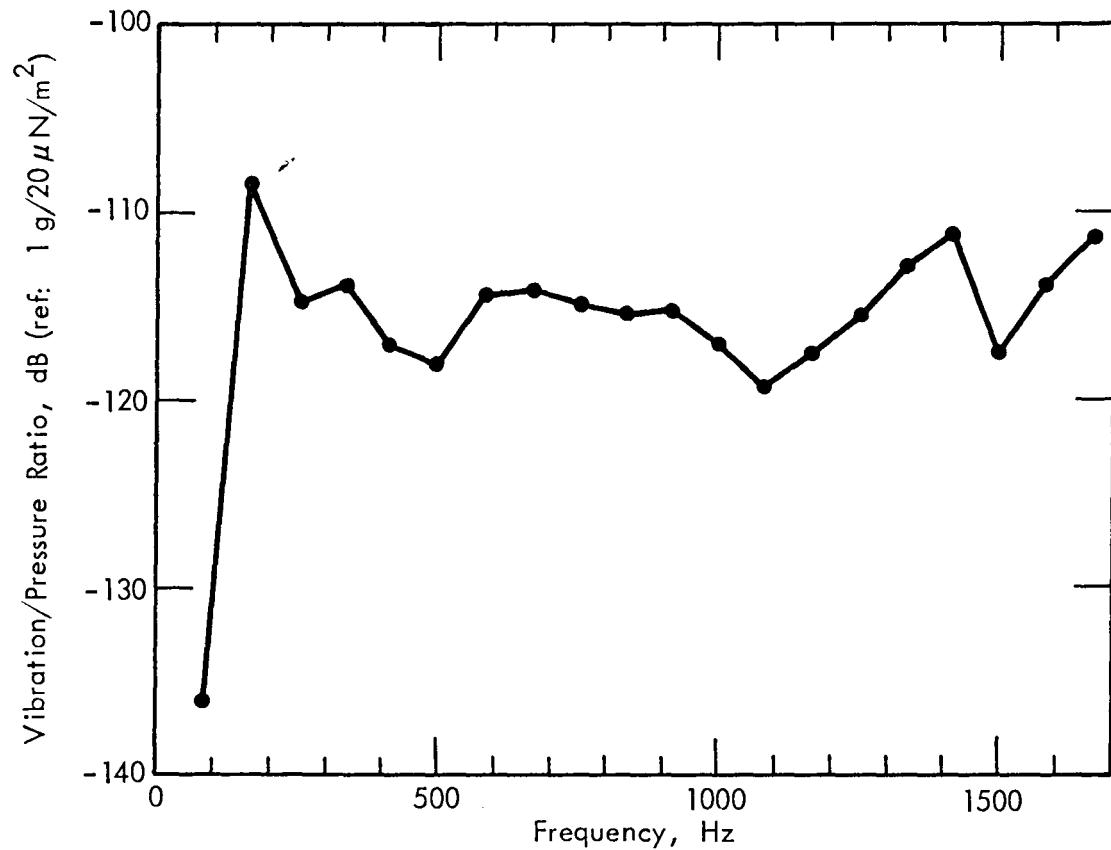
FIGURE 3.   RATIO OF PROPELLER INDUCED VIBRATION
A1 TO PRESSURE M4 FOR 2600 rpm
OPERATION

controlled response.   The results in Figure 3 generally corre-
spond to a dynamic system at this location with a basic resonance
frequency of about 160 Hz.   More detailed information concerning
the sidewall dynamics are presented in the next section.

4.2   Vibration/Pressure Frequency Response Functions

The magnitude of the frequency response (inertance) functions
between the exterior pressure excitation and the sidewall
vibration for all data pairs summarized in Table 2 are detailed
at frequencies of propeller blade passage and exhaust harmonics
in Appendix C. Typical plots of the inertance magnitude and
coherence between microphone 4 and accelerometer 1 for operation
of both engines at 2600 rpm (test run 12b) are shown in
Figure 4. Note that the inertance magnitude rises to a peak
near 160 Hz and then generally oscillates about a constant
value at higher frequencies, exactly as deduced from the
spectral values of pressure and acceleration in Section 4.1.
Further note that the coherence data peak sharply at the pro-
peller blade passage frequencies and most exhaust frequencies,
as would be expected since these are the only frequencies
where there is significant energy in the exterior pressure
excitation.

The inertance data for these locations (A1/M4), as measured at
the frequencies of propeller blade passage tones and exhaust
tones separately, are summarized for all test runs (excluding
the port engine operation per run 13) in Figure 5. Similar
data for microphone 7 and accelerometer 4 are shown in Figure 6.
Referring back to Figure 1, these two sets of results represent
inertance functions for typical fuselage sidewall panels. In
both cases, since the various runs cover a range of engine
speeds, the results provide reasonably well resolved inertance
estimates for the propeller excitation and the exhaust excitation
separately. Data for other accelerometer locations during oper-
ation of both engines at 2600 rpm (run 12b) are plotted in
Appendix C.
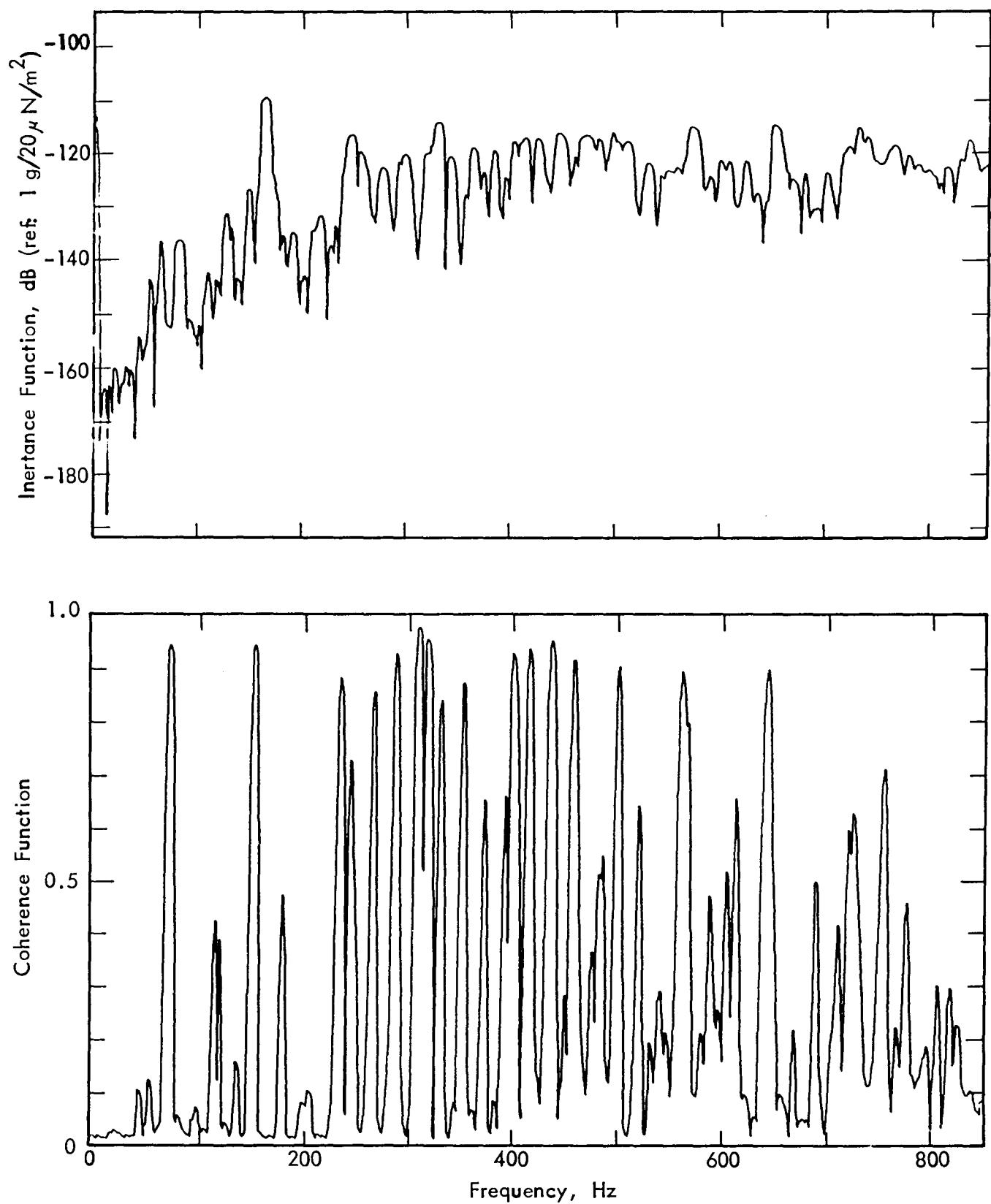
FIGURE 4. INERTANCE AND COHERENCE FUNCTIONS BETWEEN MICROPHONE 4 AND ACCELEROMETER 1 FOR 2600 rpm OPERATION
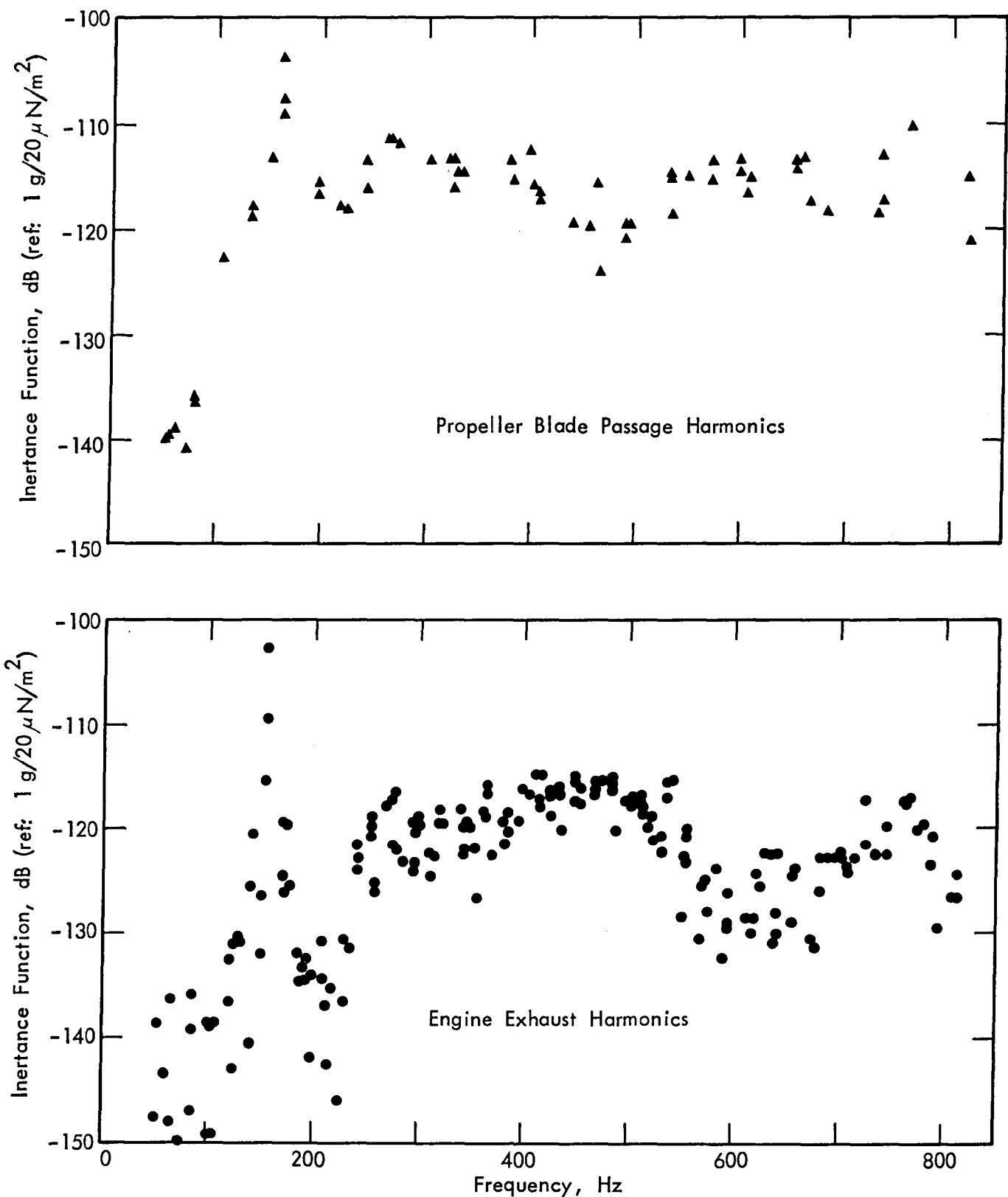
FIGURE 5.   INERTANCE FUNCTIONS BETWEEN MICROPHONE 4
AND ACCELEROMETER 1 AT PROPELLER AND EXHAUST
FREQUENCIES FOR ALL RPM OPERATIONS
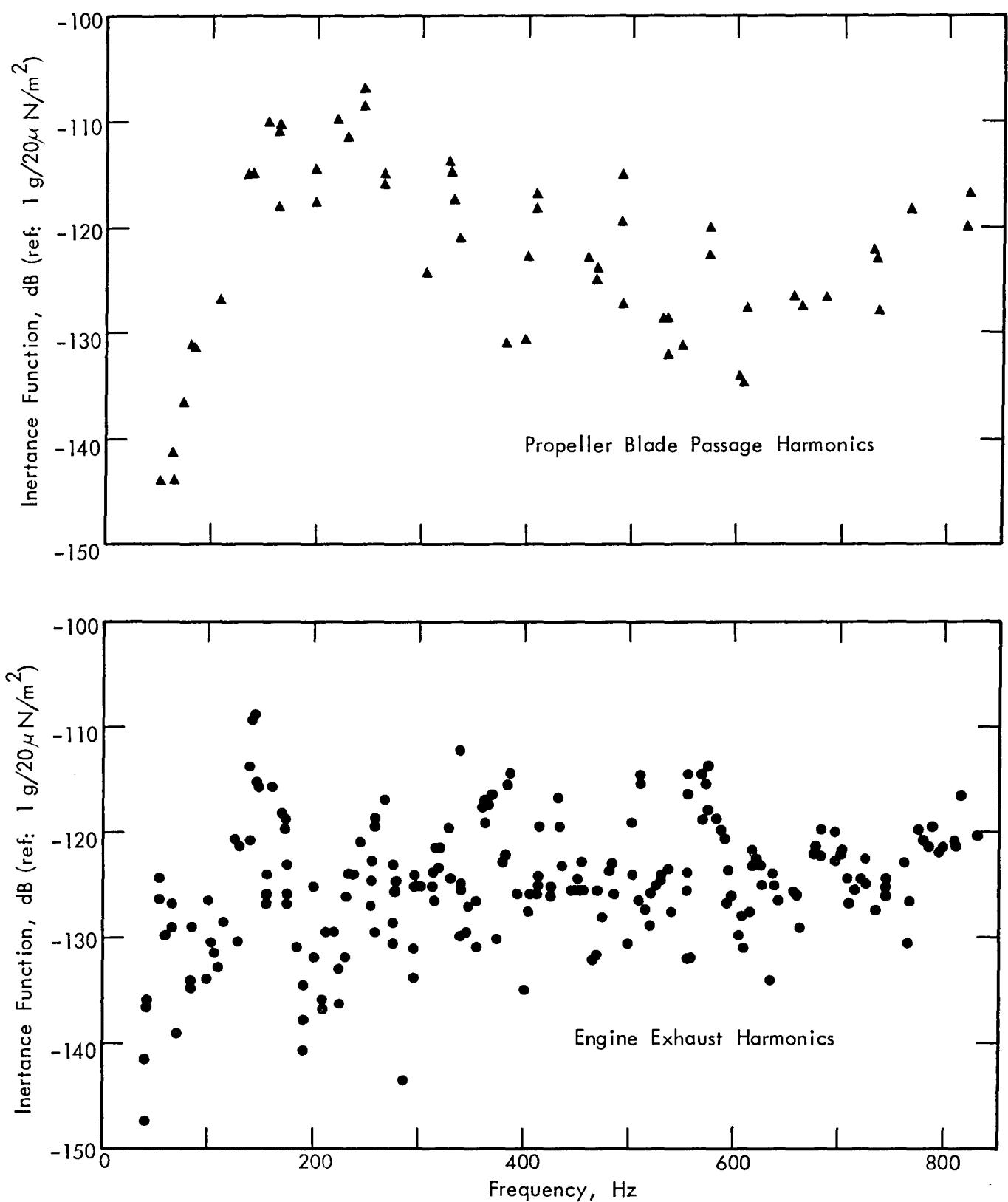
FIGURE 6. INERTANCE FUNCTIONS BETWEEN MICROPHONE 7 AND ACCELEROMETER 4 AT PROPELLER AND EXHAUST FREQUENCIES FOR ALL RPM OPERATIONS

The results with least scatter are provided by locations A1/M4 in Figure 5. Note that the inertance functions for both the propeller and exhaust excitations rise to a sharp peak at about 160 Hz with similar magnitudes of about -103 dB. This is consistent with the preliminary results in Figure 3, although the magnitude of the peak is higher here because of the better resolution. Following the peak at 160 Hz, there is a valley in the inertance function at about 220 Hz. However, the magnitude of this valley is substantially greater for the propeller excitation (about -117 dB) than for the exhaust excitation (an average of about -137 dB). The inertance functions then rise from this valley, but the propeller induced response generally remains larger at frequencies up to 300 Hz. Although there is substantially more scatter in the A4/M7 location data in Figure 6, similar relationships can be seen. The inertance peaks in the A4/M7 data occur at somewhat different frequencies reflecting the different dynamic characteristics of this panel, but the tendency for the propeller induced response to be larger at frequencies between the first peak and 300 Hz is apparent. This fact is clarified in Figure 7, which summarizes the results in Figures 5 and 6 after visual smoothing of the inertance functions due to the propeller and exhaust excitations.

The results in Figure 7 leave no doubt that the structure near the plane of the propeller accepts propeller excitation more efficiently than exhaust excitation; i.e., the joint acceptance function of the structure is larger for the propeller excitation. This clearly must be due to the spatial correlation characteristics of the two excitations. Since both excitations are basically tonal, their spatial correlations differ only in terms of trace velocity. From previous studies [1], it is known that the propeller excitation near the plane of the propeller appears to
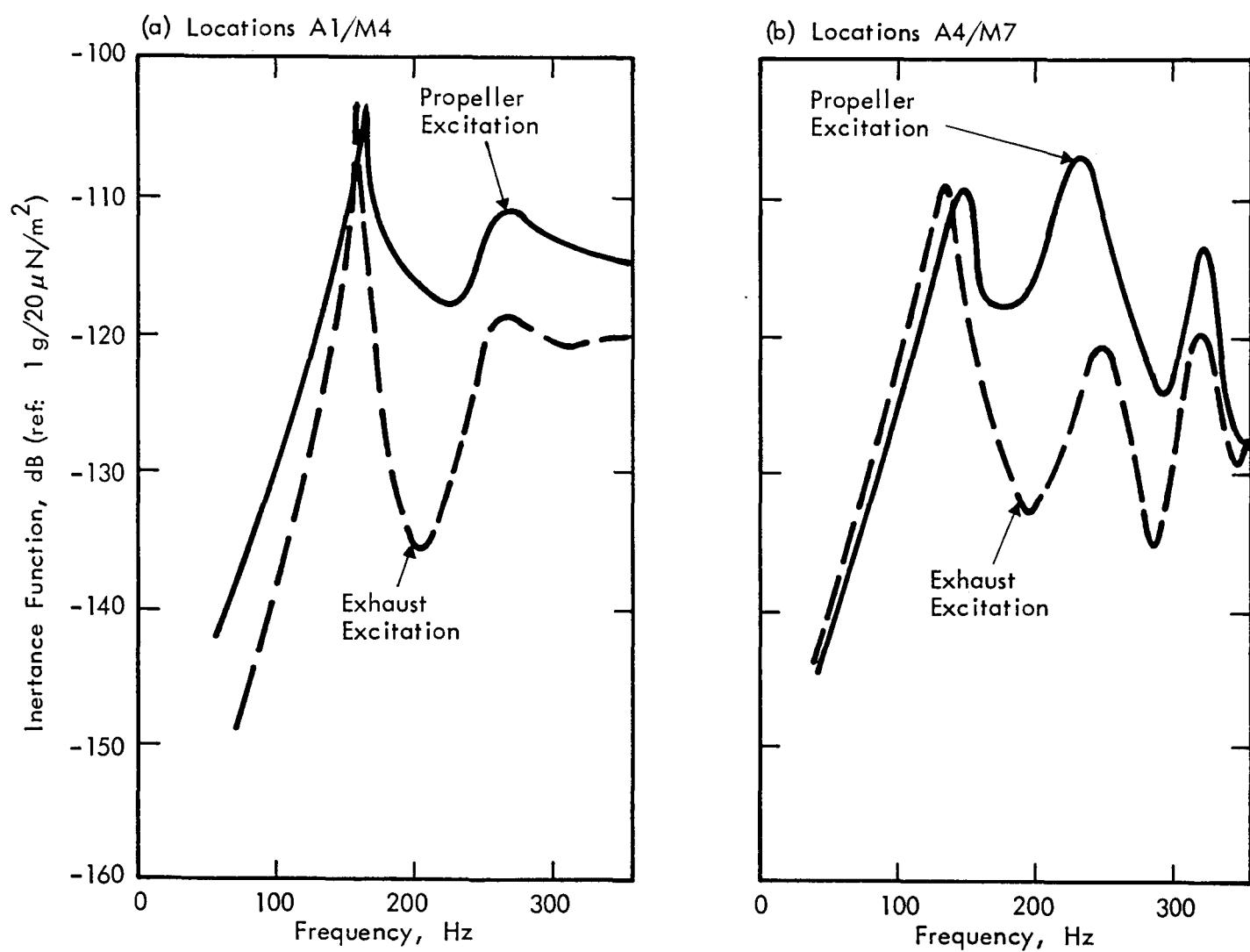
FIGURE 7. SMOOTHED INERTANCE FUNCTIONS FOR FUSELAGE SIDEWALL STRUCTURE

-23-

be aerodynamic in character, producing subsonic trace velocities
in the vertical direction and near infinite trace velocities
below 300 Hz in the longitudinal direction. On the other hand,
the exhaust excitation originates aft of the plane of the
propeller and reaches this region as an acoustic wave which
impinges on the structure with an angle of incidence of less
than 90 degrees, corresponding to a finite but supersonic trace
velocity in the longitudinal direction, as will be demonstrated
in the next section.

4.3   Phase Functions Between Spatially Separated Measurements

The calculated phase angles between the exterior pressure measure-
ment and the sidewall acceleration measurements for all data pairs
summarized in Table 3 are detailed in Appendix D. Typical results
of the phase measurements at both propeller blade passage and
exhaust frequencies for two microphone pairs, M5 versus M4 and
M5 versus M7, are shown in Figure 8. The phase data for propeller
noise only were calculated at these same locations in a previous
experiment [1]. The trace velocities indicated by the propeller
data in Figure 8 are summarized in comparison to the results
from the previous experiment in Table 6. Note that the agreement
is quite good. As before, the trace velocities for the propeller

Table 6. Trace Velocities From Pressure
Measurements For 2600 rpm Operation

Measurement	Trace Velocity, m/s	
	M5 vs. M4	M5 vs. M7
Propeller noise (current data)	206	92
Propeller noise (Ref. [1])	209	98
Exhaust noise (current data)	∞	-383

(a) Microphone 5 vs. 4 (Vertically Separated by 0.279 m)

Propeller (U_c = 206 m/s)

Exhaust ($U_c \approx \infty$)

(b) Microphone 5 vs. 7 (Longitudinally Separated by 0.368 m)

Propeller (U_c = 92 m/s)

Exhaust (U_c = 383 m/s)

Frequency, Hz
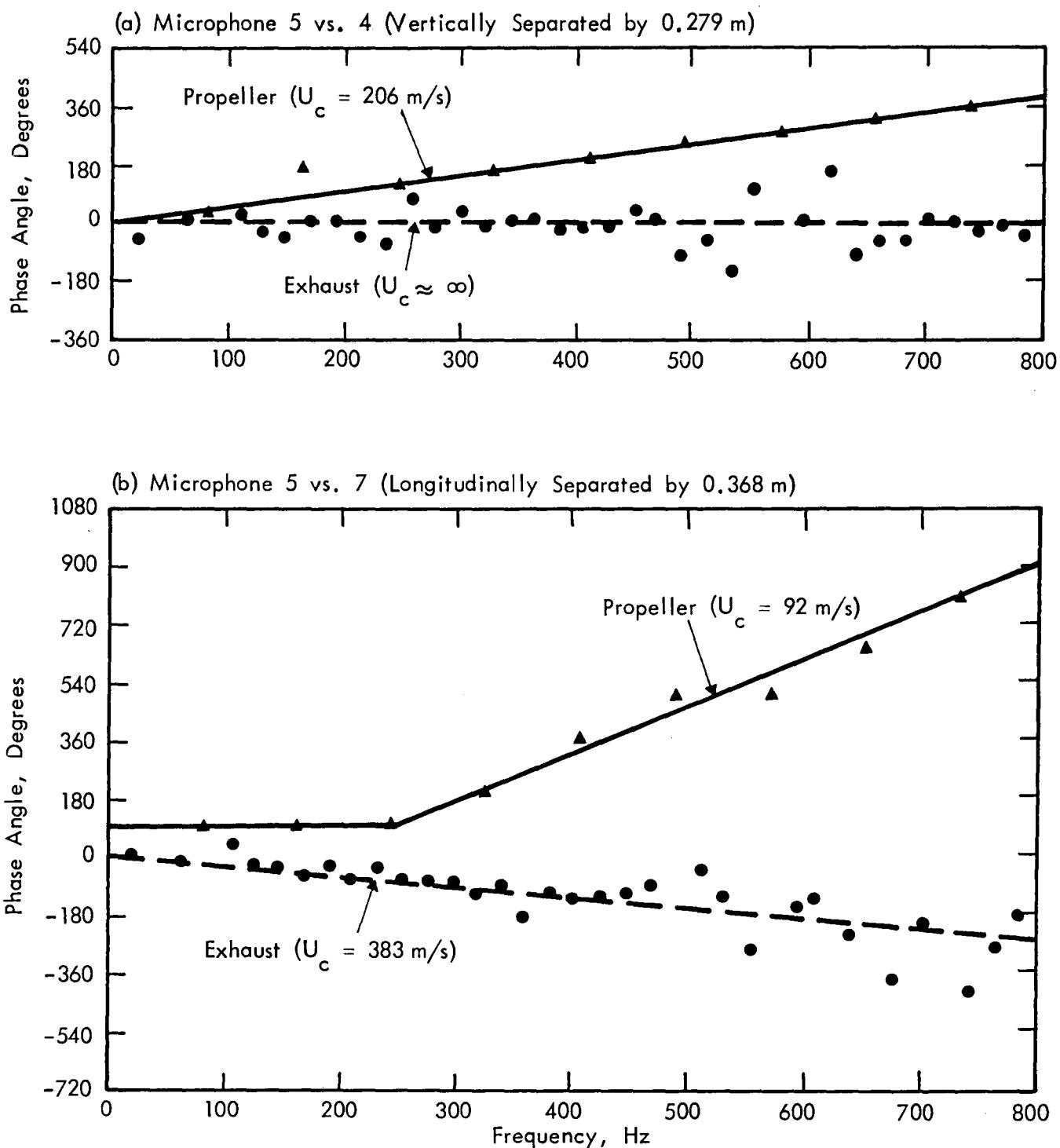
FIGURE 8.   PHASE FUNCTIONS BETWEEN VERTICALLY AND LONGITUDINALLY SEPARATED MICROPHONES FOR 2600 rpm OPERATION

noise are subsonic, suggesting the noise is aerodynamic (not acoustic) in character, as discussed in Ref. [1].

Now concerning the exhaust noise in Figure 8, the trace velocities indicated for both measurement pairs are supersonic, suggesting the exhaust noise reaches these locations as an acoustic wave. For measurement pair M5/M4, the trace velocity is near infinite, meaning the angle of incidence of the exhaust noise is about 90 degrees. This is logical since these two measurements are vertically separated with a midpoint that is approximately orthogonal to the line of sight to the exhaust. For measurements M5/M7 which are longitudinally separated, the trace velocity is about 400 m/s which corresponds to an angle of incidence of $\phi = 32°$ pointing aft. This corresponds to the approximate location of the starboard engine exhaust relative to these locations.

Also of interest here are the vibration data. Unfortunately, the phase functions for the vibration data appear to be dominated by the local resonances of the fuselage panels and, hence, reveal no definitive information concerning propagating waves. This is illustrated for the phase data between accelerometers 3 and 4 (a frame to a panel) at exhaust tone frequencies in Figure 9. Note that independent of engine speed, the phase stays at zero up to about 150 Hz, which is assumed from Section 4.2 to be first resonance frequency of this particular section. The phase then shifts abruptly to -180 degrees as would be expected in passing through a resonance.

4.4   Vibration/Acoustic Coherent Output Power Functions

The coherent output power at microphones 11 and 12 based upon the sidewall vibration measurements at the five accelerometer
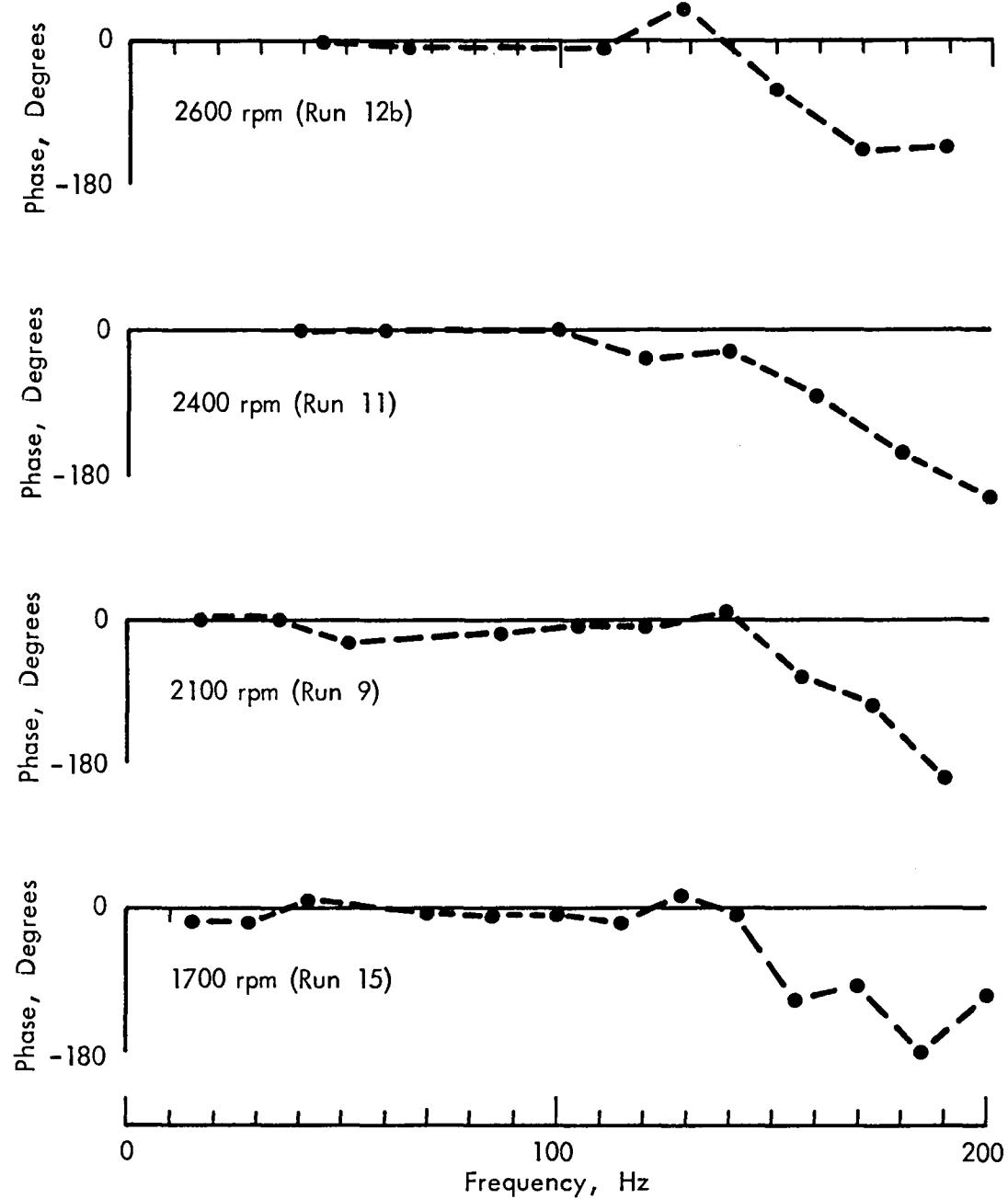
FIGURE 9. PHASE FUNCTIONS BETWEEN ACCELEROMETERS 3 AND 4 AT EXHAUST FREQUENCIES FOR VARIOUS ENGINE SPEEDS

locations in Figure 1 for both propeller blade passage and exhaust
frequencies are detailed in Appendix E. A typical plot of the
spectral and coherent output values at microphone 11 based upon
accelerometer 1 for operation of both engines at 2600 rpm (test
run 12b) are shown in Figure 10. Note that the coherent output
spectral values at most of the propeller and exhaust frequencies
are as large or almost as large as the overall spectral values.

Coherent output power calculations are fully effective in identi-
fying noise sources only when the sources are statistically
independent of one another. When two or more sources of interest
are correlated, the coherent output power at a receiver due to
any one source tends to be exaggerated [4]. When the sources
are fully correlated, the coherent output power at a receiver
due to any one source will represent the contribution of all
the sources; i.e., it will equal the overall power at the receiver
assuming no independent sources are present. For the problem
at hand, the fuselage sidewall frames and panels on the starboard
side of the airplane are all driven primarily by the starboard
engine propeller and exhaust and, hence, all vibrate at exactly
the same frequencies. Since two sine waves at identical fre-
quencies are fully correlated, the vibration response of all
points on the starboard fuselage structure are highly correlated
and their individual contributions to the interior acoustic
noise cannot be identified by coherent output power calculations.
However, because the port and starboard engines do not operate
at precisely the same speed, the relative contributions of the
noise through the port versus starboard side of the fuselage
can be identified.

To illustrate the above point, consider the interior noise levels
(M11 and M12) at the first three propeller blade passage
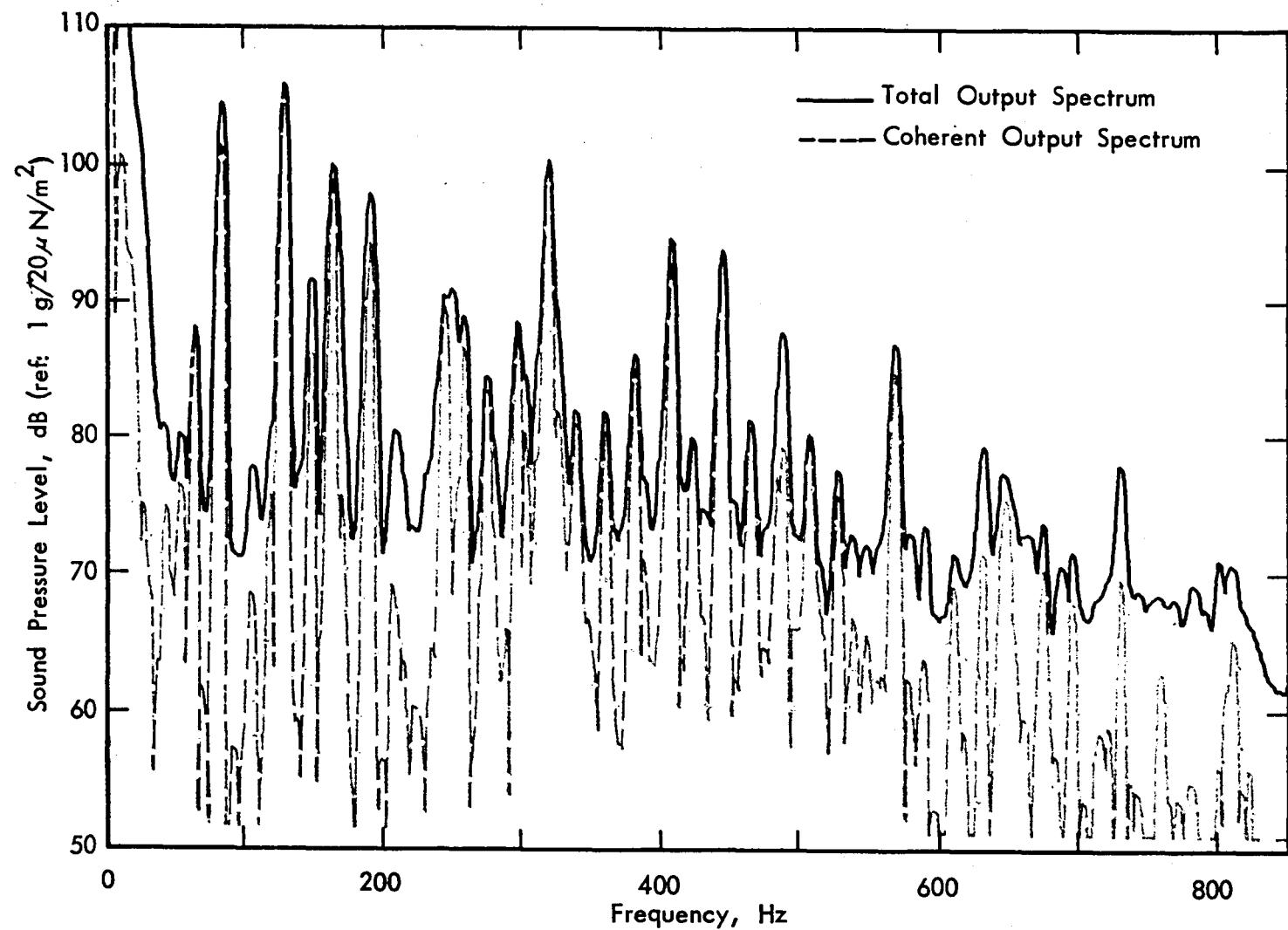
FIGURE 10. TOTAL AND COHERENT OUTPUT SPECTRUM AT MICROPHONE 11 BASED UPON ACCELEROMETER 1 FOR OPERATION AT 2600 rpm (RUN 12b)

frequencies during operation at 2100 rpm, as summarized in
Table 7. This table shows the coherent output spectral levels
at the first three propeller blade passage frequencies during
operation of both engines at 2100 rpm based upon an average of
three accelerometers (A1, A4 and A5). Since these three acceler-
ometers were on the starboard side of the fuselage, the resulting
coherent output power values should represent the contribution of
the starboard engine to the total interior noise levels. As a
check on the coherent output power results, the overall levels
measured by M11 and M12 with the starboard engine only operating
are also shown. Note that the results are in reasonable agreement.

Table 7. Comparison of Total and Coherent Output
Power for Propeller Induced Interior Noise
During Operation at 2100 rpm.

Receiver Microphone	Propeller Harmonic Order	Average* $G_{yy}(f)-G_{y:x}(f)$ From Table E-2 (dB)	Coherent Output (dB) Both (Run 9)	Spectral Values From Tables B-8 and B-9 (dB)		
				Stbd. (Run 14b)	Port (Run 13)	Both (Run 9)
M11	1	10.6	90.1	93.7	99.9	100.7
	2	0.7	96.3	96.2	86.6	97.0
	3	0.9	87.5	86.7	77.7	88.4
M12	1	0.8	105.9	106.6	100.6	106.7
	2	2.1	92.2	91.8	91.8	94.3
	3	0.5	92.2	91.5	86.8	92.7

*Average difference between the overall value and the coherent
output values measured using accelerometers A1, A4 and A5.

Of particular interest in Table 7 is the result for M11 at the
first propeller blade passage harmonic. Although M11 is on the
starboard side of the interior, the data in Appendix B (summarized

in Table 7) indicate the spectral level of the first propeller
tone at this location is due primarily to the port engine,
probably because of geometric considerations. The coherent
output power calculation detects this curious situation, as
indicated by the 10.6 dB reduction in the two engine overall
level in Table 7. There is still a 3.6 dB discrepancy between
the coherent output and spectral levels, but this can be
explained by the uncertainties caused by the propeller beat
phenomenon at this location.

Discussion of the coherent output power can be taken a little
further when the results of the beat amplitude analysis are
also taken into consideration. Results from the two approaches,
coherent output power and beat amplitude, are seen to be con-
sistent with the coherent output power having the advantage
that the method can identify the propeller making the greater
contribution to the sound level at a given microphone location.
In order to demonstrate the different methods, Table 8 combines
coherent output power data with the results taken from the beat
amplitude analysis in Table F-2.

The interesting information is contained in the last four columns
of Table 8. The coherent output power analysis provides the
difference between the measured harmonic level with both engines
operating and the coherent output power associated with the
vibration of the starboard side of the fuselage. This result is
interpreted as an indication of the contribution of the starboard
propeller to the noise level at the receiver microphone. The
beat amplitude analysis provides estimates of the difference
between the measured (total) harmonic level with both engines
operating and either the maximum or minimum contribution from the
individual propellers. It is not possible, however, to identify

Table 8. Comparison of Coherent Output Power and Beat Amplitude Analysis

Engine Speed (rpm)	Receiver Microphone	Propeller Harmonic Order	Spectrum Levels (dB)			COP* (dB)	Spectrum Level-COP (dB) (Total-Stbd)	Difference in Engine SPL (dB). See Table F-2.		Dominant Propeller (Deduced)
								Total-SPL$_{max}$	Total-SPL$_{min}$	
	Operating Engines		Stbd	Port	Both	Both	Both	Both	Both	
2100 (Runs 9, 13, & 14b)	M1	1	93.7	99.9	100.7	90.1	10.6	0.6	9.1	Port
		2	96.2	86.6	97.0	96.3	0.7	0.7	8.2	Stbd
	M2	1	106.6	100.6	106.7	105.9	0.8	1.1	6.6	Stbd
		2	92.3	91.8	94.3	92.2	2.1	1.8	4.8	Stbd
2600 (Run 12b)	M1	1	–	–	104.7	100.8	3.9	2.1	4.1	Port
		2	–	–	100.2	98.8	1.4	1.8	4.8	Stbd
	M2	1	–	–	102.5	100.5	2.0	2.1	4.1	Stbd
		2	–	–	103.1	102.6	0.5	0.9	7.4	Stbd

*This is the average value of coherent output power for accelerometers A1, A4 and A5.

which propeller is the dominant noise source.

A comparison of the two approaches shows that there is good consistency, given that the beat amplitude analysis cannot distinguish between port and starboard propellers. The results indicate that the starboard propeller is the major contributor to the sound levels at microphone location M12 for both engine speeds, and is the major contributor for the second order harmonic at microphone M11. As observed previously, the port engine is the major contributor to the first order harmonic level at microphone M11 for an engine rpm of 2100. Table 8 indicates that the same is true at 2600 rpm although the dominance of the port propeller is much reduced.

5. PREDICTION OF FREQUENCY RESPONSE FUNCTIONS

5.1 Theory

It is possible to compare the measured frequency response functions
in Figures 5 and 6 with predicted values using fairly simple
analytical models, provided that there are adequate analytical
descriptions of certain functions. One such function is the ex-
ternal pressure field which is generated by the propeller and
engine exhaust. Details of the propeller noise field have been
determined in preceding studies of the Aero Commander [1,2], and
the information can be used in this discussion. Information re-
garding the exhaust noise field is not so well defined, so that
certain assumptions have to be made.

Analysis of Aero Commander propeller noise measurements has indi-
cated [1,2] that the low order harmonic components can be con-
sidered as sinusoidal, or deterministic, while higher order har-
monics have greater random content. For the analysis of panel
frequency response functions it is assumed that the excitation
field can be considered as a deterministic, periodic pressure
plane wave propagation parallel to one axis of the panel. Then
the pressure wave will have constant phase along any direction
perpendicular to the direction of propagation. A similar repre-
sentation is assumed also for the exhaust noise pressure field.

The equation of motion for flexural response of a plate can be
written

$$M\ddot{w} + C\dot{w} + D\nabla^4 w = p(\underline{x},t) \tag{7}$$

where $w(\underline{x},t)$ is the displacement associated with a pressure
$p(\underline{x},t)$. M, C, and D represent mass, damping and stiffness of
the plate. Assuming a normal mode solution

$$w(\underline{x},t) = \sum_{\alpha=1}^{\infty} q_\alpha(t)\psi_\alpha(\underline{x}) \quad , \tag{8}$$

the modal response equation is

$$M_\alpha \ddot{q}_\alpha(t) + C_\alpha \dot{q}_\alpha(t) + K_\alpha q_\alpha(t) = L_\alpha(t) \tag{9}$$

where $L_\alpha(t)$ is the modal generalized force

$$L_\alpha(t) = \int_A p(\underline{x},t)\psi_\alpha(\underline{x})d\underline{x} \tag{10}$$

Now assume that the excitation can be represented by the general complex formulation

$$p(\underline{x},t) = p_o \exp\left[i(\omega t - kx)\right] \tag{11}$$

with the understanding that the real part of the solution will be recovered at the end of the analysis.

If Eq.(11) is substituted into Eq.(10), and the panel is assumed to have sinusoidal mode shapes associated with simply-supported boundary conditions, then

$$L_\alpha(t) = \int_0^a \int_0^b p_o \exp\left[i(\omega t - kx)\right] \sin k_m x \sin k_n y \; dy dx \tag{12}$$

where (a,b) are the panel dimensions in the (x,y) directions, α is the mode order, $\alpha \equiv (m,n)$, $k_m = m\pi/a$ and $k_n = n\pi/b$.

Now, following arguments similar to [6],

$$q_\alpha(t) = R\left\{ \frac{L_\alpha(t)}{Z_\alpha(\omega)} \right\} \tag{13}$$

where R denotes the real part of the ratio, and $Z_\alpha(\omega)$ is the modal impedance

$$Z_\alpha(\omega) = M_\alpha\left[(\omega_\alpha^2 - \omega^2) + i\eta_\alpha \omega_\alpha^2 \right] \tag{14}$$

M_α is the modal mass for mode α which has resonance frequency ω_α and loss factor η_α. (Numerically, η_α is twice the critical damping ratio).

Combining these results

$$q_\alpha(t) = 2 \, p_o \, \frac{k_m}{k_m^2 - k^2} \cdot \frac{1}{k_n} \cdot \frac{1}{|Z_\alpha(\omega)|} \left\{ \cos(\omega t - \phi_\alpha) - (-1)^m \cos(\omega t - \phi_\alpha - ka) \right\}$$

$$\text{when n odd, } k_m \neq k$$

$$= p_o \cdot \frac{a}{k_n} \cdot \frac{1}{|Z_\alpha(\omega)|} \sin(\omega t - \phi_\alpha) \quad \text{when n odd, } k_m = k$$

$$= 0 \quad \text{when n even.} \tag{15}$$

From Eq. (8) the mean square displacement is given by

$$\overline{w}^2(\underline{x}) = \underset{T \to \infty}{\text{Lim}} \frac{1}{T} \int_0^T \left[\sum_\infty q_\alpha(t) \psi_\alpha(\underline{x}) \right]^2 dt \tag{16}$$

which on substitution gives the acceleration transfer function (or inertance),

$$\frac{\overline{\ddot{w}^2}(\underline{x})}{p_o^2} = \sum_\alpha \sum_\beta \frac{\omega^4 a^2 b^2 \psi_\alpha(\underline{x})\psi_\beta(\underline{x})}{|Z_\alpha(\omega)||Z_\beta(\omega)|} \; j'_{ns}\Big(j_{mr}\cos(\phi_\beta-\phi_\alpha)-k_{mr}\sin(\phi_\beta-\phi_\alpha)\Big)$$

(17)

where $\alpha \equiv (m,n)$, $\beta \equiv (r,s)$

$$j_{mr} = \frac{2}{a^2} \quad \frac{k_m}{k_m^2-k^2} \quad \frac{k_r}{k_r^2-k^2} (1-(-1)^m \cos ka),$$

$$m+r \text{ even}, \; k\neq k_m, k\neq k_r$$

$$= \; 1/4 \qquad\qquad m=r, \text{ and } k=k_m$$

$$= \; 0 \qquad\qquad \text{otherwise,}$$

$$k_{mr} = \frac{2}{a^2} \frac{k_m}{k_m^2-k^2} \frac{k_r}{k_r^2-k^2} (-1)^m \sin ka \quad m+r \text{ odd}, \; k\neq k_m, k\neq k_r$$

$$= \frac{1}{a} \frac{k_m}{k_r^2-k_m^2} \qquad m+r \text{ odd}, \; k=k_m$$

$$= 0 \qquad\qquad m+r \text{ even}$$

and
$$j'_{ns} = \frac{2}{b^2} \cdot \frac{1}{k_n k_s} \qquad n \text{ and } s \text{ odd}$$

$$= 0 \qquad\qquad n \text{ or } s \text{ even}$$

Apart from different notations the result given in Eq. (17) is the same as that obtained in [7] where correlated progressive wave excitation was considered as a special case of a convected random pressure field. Joint terms in Eq. (17) are defined as those with m=r or n=s, and cross terms with m≠r or n≠s. Cross terms will make either positive or negative contributions to the total response.

5.2 Application to Test Panel

The structure selected for study is the panel carrying accelero-
meter Al (Figure 1). This panel is the central unit in a three-
panel array located between two windows on the starboard side of
the Aero Commander fuselage. Approximate dimensions of the panel,
based on the geometric centerlines of the adjacent frames and
stringers are,

$$a = 0.38m \ (14.75 \ in), \quad b = 0.15m \ (7.0 \ in),$$

with thickness h = 1.02 mm (0.04 in).

The measurement location (x,y) is, approximately,

$$\frac{x}{a} = 0.83, \qquad\qquad \frac{y}{b} = 0.32$$

where x is the distance aft of the forward frame of the panel,
and y is measured upward from the stringer below the panel.

Boundary conditions for the panel will lie between the extremes
of simply-supported and clamped. Resonance frequencies were
calculated for each extreme boundary condition, and the values
for a given mode order were averaged. As this approach resulted
in a frequency for the (1,1) mode which was very close to a
corresponding value calculated by Vaicaitis and Slazak (NASA
Grant NSG-1450) using transfer matrix methods for the three-panel
array, the average frequency values were used for all modes of
the panel. These values are listed in Table 9 for the frequency
range of interest (0 - 1000 Hz).

Table 9. Calculated Resonance Frequencies for Test Panel

Mode order m	1	2	3	4	5	6
Mode order n	Resonance Frequency Hz					
1	168.5	218.0	306.5	436.6	608.2	820.7
2	497.0	549.3	638.7	766.8	935.0	- -

5.2.1 Propeller Noise Excitation

In this case the measured transfer function spectrum used for comparison with the analytical results is that shown in the upper part of Figure 5. This transfer function is associated with excitation at propeller harmonic frequencies, the data being obtained over a range of propeller rotational speeds from 1700 to 2600 rpm. The pressure field trace velocity is in the y-direction, and the magnitude of the velocity varies with propeller rpm. In order to simplify the computations, an average trace velocity of 213 m/s (700 ft/sec) was assumed, corresponding to the 2400-2600 rpm conditions.

The acceleration frequency response spectrum was calculated using Eq. (17) with a trace velocity U_c of 213 m/s in the positive y-direction. Modal impedance, $Z(\omega)$, was calculated using the resonance frequencies given in Table 9 and structural loss factors of 0.01 and 0.04. The resulting predicted transfer functions are plotted in Figure 11 where they are compared with measured data taken from the upper part of Figure 5.

The calculated transfer functions in Figure 11 show contributions from six modes:- (1,1), (3,1), (5,1) (1,2), (3,2), and (5,2). Modes with even order m had zero contribution because of the assumed uniform phase of the excitation in the x-direction. Comparing measured and predicted results it is seen that the resonance peaks in the predicted spectra are not found in the measurements. When the assumed value of the structural loss factor is increased from 0.01 to 0.04 (corresponding to a change from 0.005 to 0.02 in viscous damping coefficient) the resonance peaks are reduced by 12 dB while there is little change in the level of the spectral troughs. Thus the prediction for the higher loss factor shows closer agreement with the test results.
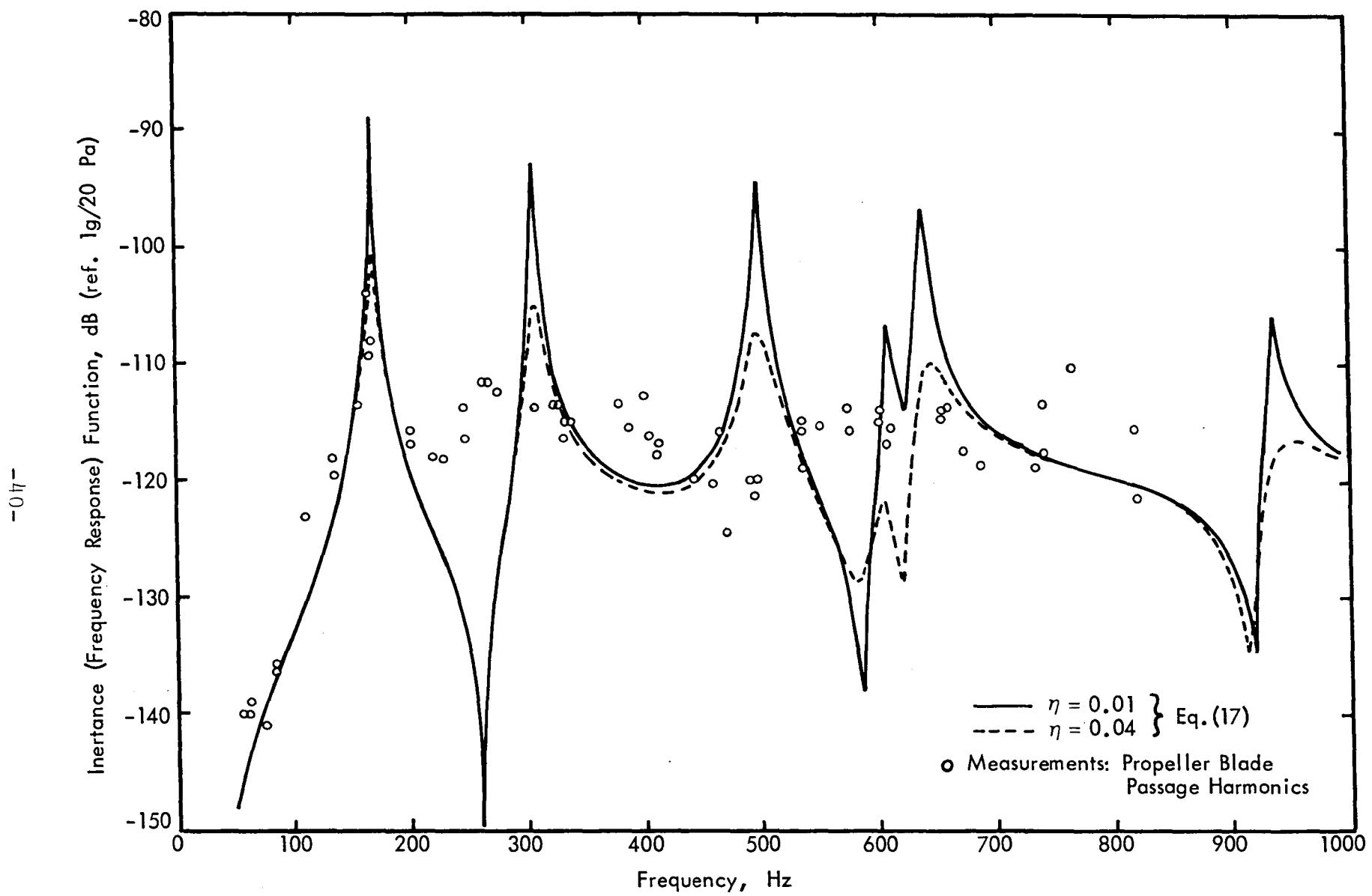
FIGURE 11. COMPARISON OF MEASURED AND PREDICTED FREQUENCY RESPONSE FUNCTIONS (MICROPHONE 4, ACCELEROMETER 1, PROPELLER NOISE EXCITATION)

-40-

The predicted spectra in Figure 11 show a strong trough at about
260 Hz. This occurs because of the negative contributions from
the crossterm associated with the mode pair (1,1) and (3,1). The
data do not show such a trough, nor do they exhibit the trough
predicted at about 580 Hz.

The experimental data presented in Figure 11 were obtained for
four different propeller rpm conditions and, thus, are associated
with four different pressure field trace velocities in the range
150 to 220 m/s. However, variations in trace velocity, within
this range, have little effect on the predicted transfer function
spectrum, as is shown in Figure 12. Furthermore, the test data
show no identifiable dependency on propeller rpm. Thus the com-
parison of results in Figure 11 should not be sensitive to the
choice of trace velocity for the predictions.

5.2.2 *Exhaust Noise Excitation*

Measured inertance data for the panel of interest and exhaust
noise excitation are contained in the lower part of Figure 5.
Predicted inertance functions for the test condition have been
calculated using Eq. (17), with the pressure field trace velocity
of 328 m/s in the negative x-direction (see Table 6). In this
case modes of even order in the y-direction will make zero contri-
bution to the predicted panel response.

The comparison between predicted and measured transfer functions
for exhaust noise excitation is shown in Figure 13. As was the
case for propeller noise, the test data do not show the spectral
peaks predicted by the simple model except, perhaps, for the (1,1)
mode. In general there is closer agreement between experimental
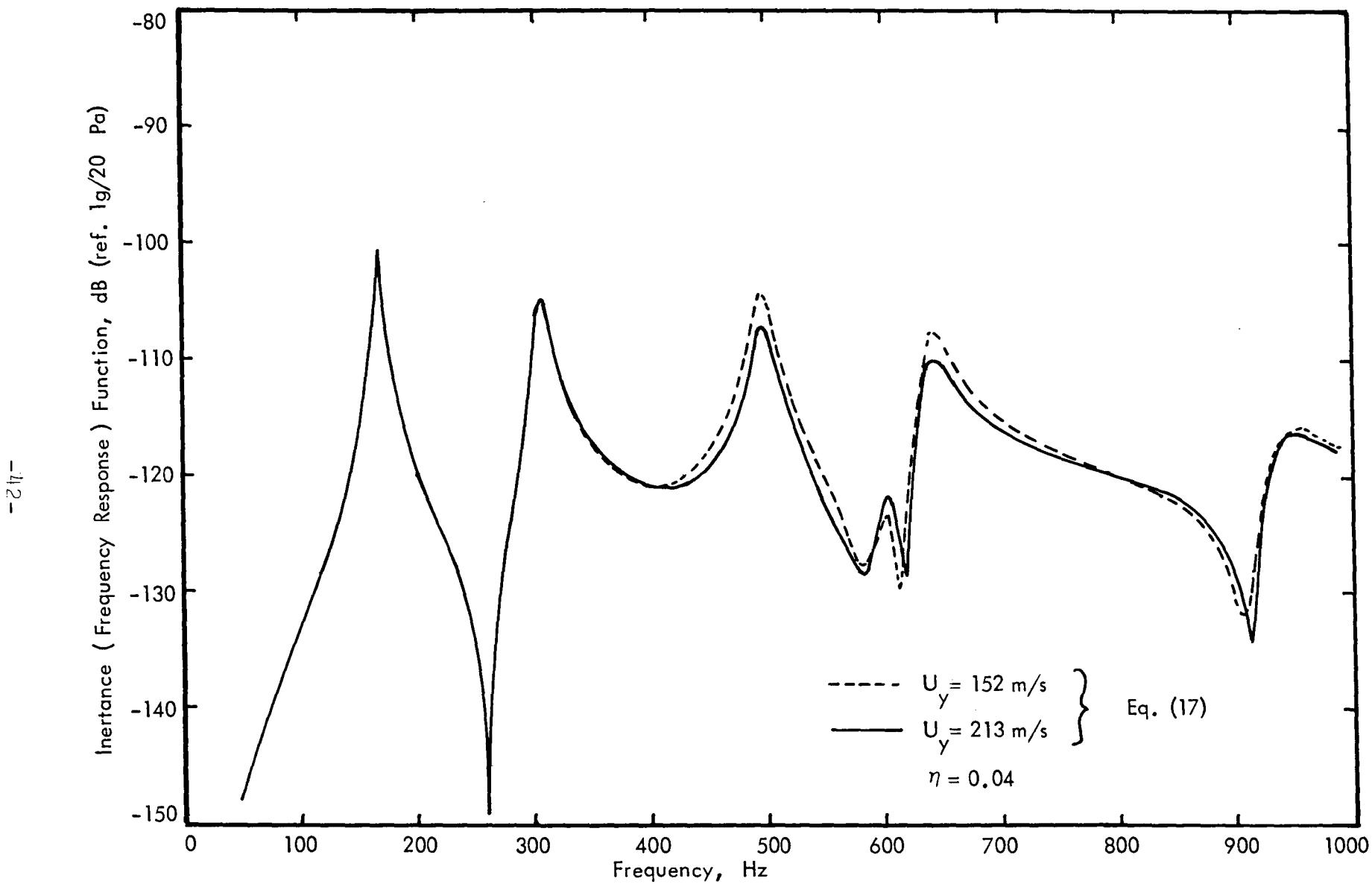
FIGURE 12. EFFECT OF TRACE VELOCITY ON PREDICTED FREQUENCY RESPONSE FUNCTION (MICROPHONE 4, ACCELEROMETER 1, PROPELLER NOISE EXCITATION)
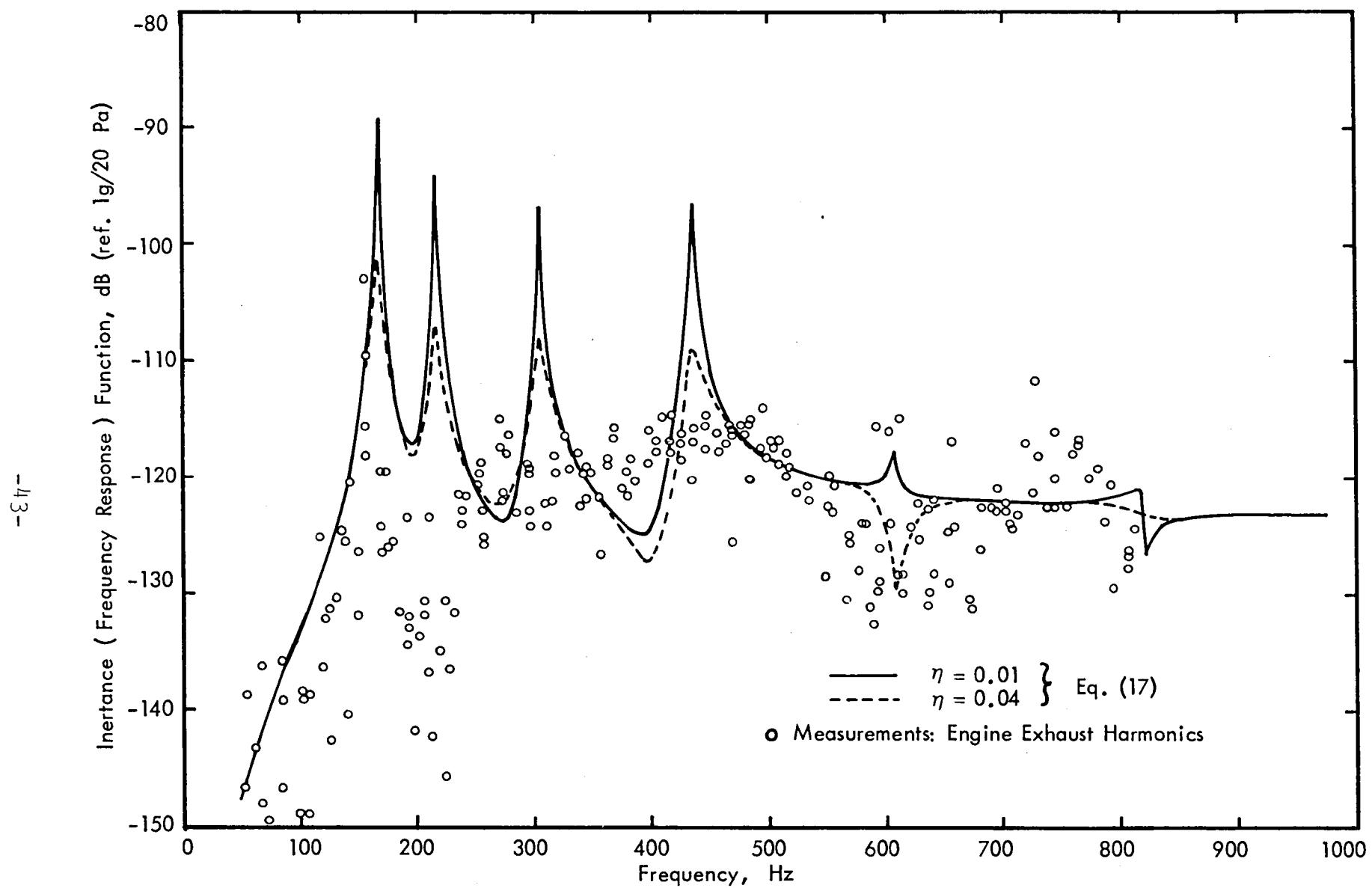
FIGURE 13. COMPARISON OF MEASURED AND PREDICTED FREQUENCY RESPONSE FUNCTIONS (MICROPHONE 4, ACCELEROMETER 1, ENGINE EXHAUST NOISE EXCITATION)

and predicted results when the higher loss factor of 0.04 is assumed. Furthermore the agreement is best at frequencies above about 230 Hz.

5.3 Discussion

There are several possible reasons for the lack of close agreement between the measured and predicted transfer functions shown in Figures 11 and 13. These reasons include:

(a) assumed damping loss factor may be incorrect

(b) assumed mode shapes may not provide an accurate-enough representation of the actual shapes

(c) excitation may not be described in sufficient detail

(d) panel should not be considered in isolation with respect to adjacent structure.

If the structural loss factors were to be increased from 0.04 to 0.10 for all modes except (1,1) the resonance peaks would begin to merge into the broadband levels. However, $\eta = 0.10$ is a high value for the loss factor. Measurements of damping for typical fuselage structures of general aviation aircraft are needed as a data bank for calculations of this type. These measurements would indicate whether or not η should be frequency (or mode) dependent.

Errors in assumed mode shape would influence the calculated joint and cross acceptance terms (j_{mr}, k_{mr} and j'_{ns}). Also they would influence the modal response at a given point $\underline{x}$ because this response is very sensitive to the location of nearby node lines. Idealization of the panel as an isolated structure limits the number of modes which participate in the response calculations.

As a consequence the predicted spectra show a series of strong, well-separated, peaks. If a larger structural region, with more modes, was used as the structural model, the resulting predicted spectrum would have a larger number of peaks which would merge into one another.

In spite of the areas of uncertainty and the use of a simplified analytical approach, the general agreement between predicted and measured results in Figures 11 and 13 is quite good. This is a fairly early step in the development of a good understanding of general aviation aircraft fuselage response to propeller noise.

6.0 CONCLUDING REMARKS

Analysis of vibration and acoustic data associated with
static operations has provided some information regarding the
response of the fuselage to propeller and exhaust noise excita-
tion. Measurements of the propeller noise field on the exterior
of the fuselage have been analyzed in two preceding reports [1,2],
thus the present concluding remarks are directed towards the
fuselage vibration and interior noise results. It should be
recognized, however, that some of the conclusions are tentative
because of the small number of measurement locations.

On the basis of the five accelerometer locations, the fuselage
skin panels near the plane of rotation of the propeller appear
to accept propeller noise excitation more efficiently than they
accept exhaust noise. However the frame and longeron results
indicate significant contributions from exhaust noise excitation.
This may be due to propagation from other structural regions;
further measurements would be required before such a conclusion
could be accepted with confidence. Interior noise spectra show
contributions from both propeller and exhaust noise and, on the
basis of the available vibration data, it seems likely that the
two noise components have different transmission paths into the
cabin.

It has been shown previously [2] that propeller noise levels in
the cabin, measured in the plane of rotation of the propellers,
varied with forward speed of the airplane. This has been inter-
preteted as showing that propeller noise during static operations
is transmitted into the cabin over a wide structural region.
Analysis of the present test results was not able to confirm the
above interpretation because of the limited spatial extent of the

accelerometer array. The same limited transducer array also prevented analysis of the data in terms of flexural wave propagation in the structure.

Coherent output power measurements relating structural vibration and cabin noise level could distinguish between the contributions from the right and left hand propellers as they occurred at slightly different frequencies. However the measurements were not able to identify the relative roles played by skin panels, stiffeners and window pane in transmitting sound from the exterior because all structures were exposed to the same sinusoidal excitation.

Measured inertance (frequency response) functions associated with fuselage panel response to propeller and exhaust noise excitation show broadband-type characteristics without many strong peaks associated with resonance. Simplified analysis shows reasonably good agreement with measured data except at predicted resonance frequencies. The agreement is improved if fairly high values of structural damping are assumed for the analytical model, although there is no direct experimental justification for making the assumptions.

In conclusion, the vibration and interior noise test data have provided useful information regarding fuselage response to propeller and exhaust noise excitation. However, a more-extensive experimental and analytical program is required before a full understanding of the noise transmission paths into the cabin can be established.

REFERENCES

1. A. G. Piersol, E. G. Wilby, and J. F. Wilby, "Evaluation of Aero Commander Propeller Acoustic Data: Static Operations", NASA CR-158919, May 1978.

2. A. G. Piersol, E. G. Wilby, and J. F. Wilby, "Evaluation of Aero Commander Propeller Acoustic Data: Taxi Operations", NASA CR-159124, July 1979.

3. J. T. Howlett and J. A. Schoenster, "An Experimental Study of Propeller-Induced Structural Vibration and Interior Noise", SAE Paper 790625, April 1979.

4. J. S. Bendat, "Statistical Errors in Measurement of Coherence Functions and Input/Output Quantities", *Journal of Sound and Vibration*, Vol. 59, pp 405-421, 1978.

5. J. S. Bendat and A. G. Piersol, *Random Data: Analysis and Measurement Procedures*, Wiley-Interscience, New York 1971.

6. *Noise and Acoustic Fatigue in Aeronautics*, Chap.13, "Elements of Periodic Vibration Theory", Editors E. J. Richards, D. J. Mead, John Wiley and Sons Ltd., 1968.

7. Wilby, J. F. "The Response of Simple Panels to Turbulent Boundary Layer Excitation", AFFDL-TR-67-70 October 1967.

APPENDIX A

Frequencies of Propeller Blade Passage and
Exhaust Harmonics For All Test Runs

Table A-1. Frequencies of Propeller Blade Passage and Exhaust Harmonics For All Test Runs

Engine rpm		1700	2100			2400	2600	
Run Number		15	9	13	14b	11	12	12b
Operating Engines		Stbd	Both	Port	Stbd	Both	Both	Both
Harmonic Order		Harmonic Frequency, Hz						
Propeller	Exhaust							
	1	14	17	17	17	20	21	21
	2	28	35	35	35	40	42	42
	3	42	52	52	52	60	64	64
1	-	*55*	*66*	*67*	*67*	*76*	*82*	*82*
	4	57	69	70	69	79	85	85
	5	71	86	87	87	99	106	106
	6	86	104	105	104	119	128	128
	7	100	121	122	121	139	149	149
2	-	*110*	*133*	*134*	*134*	*153*	*164*	*164*
	8	114	138	140	139	160	170	170
	9	128	156	157	156	179	191	191
	10	142	173	175	174	198	213	213
	11	156	190	192	191	218	234	234
3	-	*165*	*199*	*202*	*200*	*229*	*245*	*246*
	12	171	208	210	209	238	255	256
	13	186	225	227	226	258	276	277
	14	200	242	245	243	278	298	299
	15	214	260	262	261	298	319	320
4	-	*220*	*266*	*269*	*267*	*306*	*327*	*328*
	16	229	277	280	278	318	340	341
	17	243	294	297	295	337	361	362
	18	257	311	315	312	357	383	384
	19	271	329	332	330	377	404	405
5	-	*275*	*332*	*336*	*334*	*382*	*409*	*410*

Table A-1 (Continued)

Engine rpm		1700	2100			2400	2600	
Run Number		15	9	13	14b	11	12	12b
Operating Engines		Stbd	Both	Port	Stbd	Both	Both	Both
Harmonic Order		Harmonic Frequency, Hz						
Propeller	Exhaust							
	20	286	346	350	347	397	425	426
	21	300	363	368	364	417	447	448
	22	314	381	385	383	437	468	469
	23	329	396	403	400	457	489	490
6	-	330	397	403	401	458	491	492
	24	343	415	420	418	476	510	511
	25	357	433	438	436	496	532	533
	26	372	450	455	453	516	553	554
7	-	385	463	470	468	535	573	574
	27	386	466	472	470	537	575	576
	28	400	484	490	487	556	595	597
	29	414	502	508	505	576	617	619
	30	429	519	525	522	596	638	640
8	-	440	530	538	534	611	654	656
	31	443	536	543	540	615	659	661
	32	457	554	560	557	635	680	682
	33	472	571	578	575	655	702	704
	34	486	588	595	592	675	723	725
9	-	495	596	605	601	688	736	738
	35	400	606	613	610	695	744	746
	36	514	623	630	627	715	765	767
	37	529	640	648	644	734	787	789
	38	543	657	665	661	754	808	810
10	-	550	662	672	668	764	818	820

APPENDIX B

Vibration and Acoustic Pressure Levels
at Propeller Blade Passage Frequencies

Table B-1. Sidewall Vibration Response at Propeller
Blade Passage Frequencies - Location A1

Engine rpm	1700	2100 rpm			2400	2600 rpm	
Run Number	15	9	13	14b	11	12	12b
Operating Engines	Stbd	Both	Port	Stbd	Both	Both	Both
Harmonic Order*	Vibration Acceleration in dB (ref: 1 g)						
1	-14.8	-9.8	-20.9	-10.2	-7.8	-0.7	-1.3
2	- 1.5	+6.9	-21.6	+ 6.9	+15.4	+22.8	+22.0
3	12.3**	+4.7	-37.3	+ 4.3	+ 6.4	+13.6	+11.5
4	- 5.2	+6.8	-30.2	+ 6.4	+ 9.6	+11.4	+11.2
5	- 1.5	+1.0	-35.8	+ 1.7	+ 7.9	+ 5.8	+ 4.7
6	- 6.1	+1.5	-32.8	- 2.2	- 1.1	+ 3.4	+ 2.7
7	- 9.7	-1.1	-31.0	- 7.4	+ 0.1	+ 2.2	+ 3.0
8	-14.9	-5.5	-40.9	- 5.9	- 2.7	+ 1.2	+ 1.7
9	-11.3	-7.8	-43.5	- 7.8	- 4.9	+ 0.3	- 3.5
10	-17.3	-9.7	-44.6	-10.6	- 1.4	- 3.4	- 5.2
11	-20.3	-9.2	-43.3	-13.9	- 6.1	- 7.0	- 5.0
12	-19.9	-10.8	-47.1	-16.0	- 8.0	-11.6	- 9.0
13	-22.9	-13.0	-38.7	-14.7	-13.9	-13.3	-13.0
14	-20.6	-15.2	-40.9	-16.7	-14.4	-13.5	-15.8
15	-23.5	-22.5	-53.0	-23.8	-17.5	-12.8	-15.0
16	-24.7	-23.8	-51.8	-24.3	-16.8	-11.5	-15.4
17	-26.9	-24.0	-46.9	-26.7	-17.0	-11.7	-13.7
18	-33.6	-20.2	-48.6	-22.4	-12.6	-20.5	-22.7
19	-34.3	-17.0	-48.1	-23.4	-22.4	-19.3	-19.3
20	-35.9	-16.3	-45.3	-23.8	-23.2	-17.5	-19.0
Overall	12.5	+12.3	-17.4	+11.8	+17.7	+23.8	+22.9

* See Appendix A for frequencies.
** Possibly contaminated by exhaust noise.

Table B-2. Sidewall Vibration Response at Propeller Blade Passage Frequencies - Location A2

Engine rpm	1700	2100			2400	2600	
Run Number	15	9	13	14b	11	12	12b
Operating Engines	Stbd	Both	Port	Stbd	Both	Both	Both
Harmonic Order*	Vibration Acceleration in dB (ref: 1 g)						
1	-22.1	-16.7	-24.7	-17.9	-13.6	- 3.4	- 3.8
2	-10.2	- 8.6	-30.5	- 8.5	- 5.2	- 3.8	- 3.5
3	-27.6	-16.7	-42.1	-18.1	-21.9	-16.6	-16.7
4	-28.4	-19.9	-42.4	-24.4	-16.1	-14.2	-14.9
5	-31.3	-28.4	-45.6	-29.3	-23.8	-17.7	-18.3
6	-29.9	-23.4	-46.2	-21.7	-16.1	-14.7	-15.3
7	-29.0	-20.6	-43.5	-20.4	-18.8	-17.4	-20.0
8	-27.0	-26.1	-51.7	-27.4	-22.7	-23.1	-21.8
9	-35.6	-27.1	-50.3	-27.4	-27.1	-24.8	-24.9
10	-40.3	-31.2	-51.6	-30.5	-20.0	-22.1	-25.5
11	-35.9	-32.4	-51.5	-32.3	-27.2	-25.8	-24.1
12	-42.2	-29.2	-52.3	-32.3	-30.1	-29.1	-31.5
13	-42.1	-35.8	-52.9	-36.4	-33.6	-30.9	-32.3
14	-39.7	-34.9	-53.3	-35.7	-37.8	-34.2	-32.4
15	-43.6	-38.3	-46.0	-36.2	-35.9	-31.3	-34.5
16	-44.9	-42.3	-52.4	-39.2	-35.8	-32.5	-34.2
17	-45.6	-42.6	-59.2	-41.2	-39.8	-32.4	-32.5
18	-49.3	-41.8	-55.9	-41.4	-38.9	-28.6	-33.1
19	-51.9	-41.6	-59.7	-45.2	-34.7	-26.9	-28.7
20	-52.8	-42.3	-58.2	-44.9	-32.8	-31.0	-31.4
Overall	- 9.6	- 6.7	-23.4	- 7.0	- 3.5	- 0.1	- 0.03

* See Appendix A for frequencies.

Table B-3. Sidewall Vibration Response at Propeller
Blade Passage Frequencies - Location A3

Engine rpm	1700	2100			2400	2600	
Run Number	15	9	13	14b	11	12	12b
Operating Engines	Stbd	Both	Port	Stbd	Both	Both	Both
Harmonic Order*	Vibration Acceleration in dB (ref: 1 g)						
1	-24.0	-15.7	-33.1	-17.0	- 9.5	- 2.8	- 3.0
2	-14.9	-12.2	-38.2	-11.8	-11.0	-14.6	-15.1
3	-23.7	-15.2	-34.2	-17.3	- 9.5	- 2.3	- 2.0
4	-21.8	-13.9	-39.8	-15.1	-13.1	-12.6	-12.5
5	-28.0	-23.8	-36.2	-24.5	- 6.2	- 6.2	- 5.8
6	-29.8	-16.5	-28.0	-16.5	-13.8	-13.5	-13.9
7	-24.1	-21.9	-40.5	-21.4	-20.0	-11.4	-10.4
8	-28.2	-32.8	-46.9	-30.7	-24.9	-25.4	-25.3
9	-36.9	-25.9	-43.2	-27.4	-26.4	-19.1	-18.6
10	-34.5	-34.7	-47.3	-30.5	-21.1	-20.9	-17.7
11	-34.4	-30.1	-44.8	-28.6	-23.8	-23.3	-21.4
12	-42.3	-29.1	-40.2	-27.1	-27.8	-23.2	-24.4
13	-40.5	-30.4	-38.0	-30.8	-27.7	-18.7	-22.4
14	-37.5	-30.9	-42.4	-31.8	-25.8	-20.2	-20.6
15	-38.2	-33.9	-40.4	-32.9	-23.2	-23.1	-23.8
16	-41.3	-31.5	-39.4	-30.1	-27.3	-16.6	-20.8
17	-42.0	-29.8	-48.4	-26.8	-22.4	-19.2	-23.8
18	-43.8	-34.6	-46.8	-31.4	-23.6	-22.2	-23.7
19	-43.9	-30.5	-45.3	-29.1	-23.6	-22.3	-23.6
20	-41.6	-27.2	-46.2	-26.6	-26.9	-23.4	-25.7
Overall	-12.4	- 6.9	-24.2	- 7.3	- 1.6	+ 2.2	+ 2.3

*See Appendix A for frequencies

Table B-4. Sidewall Vibration Response at Propeller Blade Passage Frequencies - Location A4

Engine rpm	1700	2100			2400	2600	
Run Number	15	9	13	14b	11	12	12b
Operating Engines	Stbd	Both	Port	Stbd	Both	Both	Both
Harmonic Order*	Vibration Acceleration in dB (ref: 1 g)						
1	-20.0	-14.1	-36.4	-16.7	- 5.5	+ 1.3	+ 1.4
2	-10.7	+ 2.9	-23.8	+ 4.2	+12.1	+12.4	+12.9
3	-10.0	- 3.3	-29.8	- 4.4	+ 6.4	+12.2	+11.7
4	- 8.3	- 3.5	-30.2	- 6.0	- 7.1	- 1.6	- 1.7
5	-14.6	-13.3	-31.2	-11.9	-14.6	- 1.7	- 2.8
6	-20.3	-13.0	-29.6	-16.7	- 8.4	- 5.4	- 4.5
7	-22.0	-13.4	-32.4	-12.1	-16.6	- 9.7	- 9.2
8	-23.0	-22.8	-48.2	-19.5	-20.3	-13.8	-14.6
9	-26.4	-23.9	-43.4	-26.3	-16.4	-13.5	-16.8
10	-34.7	-24.2	-49.0	-23.6	-11.8	-13.3	-11.9
11	-34.2	-21.9	-40.9	-22.4	-19.6	-20.5	-20.5
12	-34.3	-21.3	-39.8	-21.7	-23.3	-24.8	-24.0
13	-31.9	-23.8	-36.6	-25.3	-26.0	-24.3	-26.7
14	-28.8	-31.1	-35.3	-29.3	-29.0	-20.6	-23.6
15	-32.8	-31.8	-46.3	-33.3	-24.8	-19.2	-23.7
16	-37.3	-34.5	-47.6	-28.7	-25.4	-19.2	-23.3
17	-40.2	-30.3	-43.7	-23.5	-25.0	-20.5	-24.9
18	-43.3	-30.3	-46.6	-27.5	-26.3	-22.5	-26.4
19	-44.5	-29.6	-46.4	-27.0	-27.3	-21.7	-26.1
20	-40.8	-31.3	-50.0	-31.8	-28.2	-24.6	-27.9
Overall	- 3.9	+ 4.9	-20.1	+ 5.4	+13.3	+15.7	+15.7

*See Appendix A for frequencies

Table B-5. Sidewall Vibration Response at Propeller
Blade Passage Frequencies - Location A5

Engine rpm	1700	2100			2400	2600	
Run Number	15	9	13	14b	11	12	12b
Operating Engines	Stbd	Both	Port	Stbd	Both	Both	Both
Harmonic Order*	Vibration Acceleration in dB (ref: 1 g)						
1	- 6.2	+ 0.5	-14.7	+ 0.2	11.4	16.2	15.6
2	- 1.2	+ 2.1	-14.8	+ 1.6	12.9	14.3	13.5
3	- 1.2	+ 4.1	-33.3	+ 3.5	6.0	3.6	2.8
4	- 7.3	- 8.5	-36.5	- 8.6	- 8.9	- 5.3	- 5.5
5	-23.6	-12.0	-33.0	- 8.7	- 5.2	- 2.8	- 3.0
6	-15.0	-14.6	-31.9	- 8.4	-14.2	-11.7	-11.9
7	-19.0	-22.1	-32.9	-17.7	-18.5	-13.5	-12.8
8	-25.1	-23.4	-46.3	-24.4	- 9.9	-12.8	-11.2
9	-28.2	-15.0	-42.4	-17.4	-11.9	-12.7	-11.8
10	-31.3	-19.9	-46.8	-17.7	- 9.9	-16.8	-14.4
11	-26.2	-22.8	-44.7	-19.8	-15.7	-17.6	-19.8
12	-28.5	-24.7	-43.6	-24.8	-15.6	- 7.5	- 7.1
13	-28.2	-27.0	-50.0	-24.1	-11.0	-16.3	-15.0
14	-26.7	-23.6	-43.0	-25.6	-18.6	-16.5	-15.7
15	-34.1	-18.5	-48.9	-20.0	-19.0	-14.6	-13.9
16	-37.0	-27.0	-51.8	-27.0	-17.4	-14.3	-16.2
17	-35.0	-28.9	-51.4	-28.6	-13.7	-25.8	-26.0
18	-28.7	-26.0	-57.3	-27.1	-26.3	- 8.3	-26.9
19	-32.3	-22.6	**	-26.7	-28.5	-28.3	-27.6
20	-41.0	-27.7	**	-32.8	-36.3	-24.0	-26.9
Overall	+ 3.0	+ 7.5	-11.6	+ 7.2	+15.8	+18.6	+17.9

 * See Appendix A for frequencies.
**No spectral peak for inadequate coherence

Table B-6. Exterior Fluctuating Pressure at Propeller Blade Passage Frequencies - Location M4

Engine rpm	1700	2100			2400	2600	
Run Number	15	9	13	14b	11	12	12b
Operating Engines	Stbd	Both	Port	Stbd	Both	Both	Both
Harmonic Order*	Fluctuating Pressure in dB (ref: 20μN/m²)						
1	125.1	129.3	102.4	129.6	133.3	135.2	135.3
2	121.4	124.5	94.0	125.9	129.0	130.6	131.1
3	116.0	120.0	80.3	121.1	124.7	127.0	127.4
4	112.7	118.2	83.1	118.0	122.8	125.0	125.0
5	110.6	116.0	77.4	115.9	120.9	122.5	122.2
6	108.2	113.7	83.6	112.4	117.8	121.2	120.8
7	105.2	112.4	77.5	110.4	115.6	117.5	116.8
8	102.7	109.3	72.6	107.0	111.1	115.7	115.7
9	99.9	106.0	70.7	104.6	110.5	113.3	112.7
10	97.1	103.7	63.9	103.8	106.5	110.9	111.5
11	94.6	101.3	66.1	99.1	106.4	109.5	109.1
12	91.8	99.6	71.9	99.6	103.3	107.0	106.7
13	89.7	96.3	73.3	95.7	101.5	105.8	106.0
14	87.7	95.5	75.2	95.3	99.8	103.6	102.3
15	85.0	93.7	67.5	91.3	97.8	102.1	101.4
16	83.1	92.0	71.5	90.4	95.7	100.3	98.2
17	81.0	91.3	75.6	88.7	94.8	98.2	98.9
18	80.2	90.1	65.9	86.3	93.6	96.7	95.0
19	80.1	91.1	68.2	88.2	91.5	94.9	93.9
20	78.9	91.3	70.4	85.7	90.9	94.2	92.1
Overall	127.4	131.5	103.2	132.0	135.7	137.6	137.8

*See Appendix A for frequencies.

Table B-7. Exterior Fluctuating Pressure at Propeller
Blade Passage Frequencies - Location M5

Engine rpm	1700	2100			2400	2600	
Run Number	15	9	13	14b	11	12	12b
Operating Engines	Stbd	Both	Port	Stbd	Both	Both	Both
Harmonic Order*	Fluctuating Pressure in dB (ref: 20μN/m²)						
1	121.9	126.7	100.0	126.7	130.6	132.6	132.3
2	115.7	119.5	78.6	119.8	123.0	124.6	124.1
3	111.5	116.3	88.2	116.4	119.8	122.0	121.8
4	107.6	113.5	79.4	111.7	116.5	119.1	119.4
5	104.0	109.5	79.5	110.0	114.5	115.9	116.1
6	102.5	105.1	83.1	107.0	111.9	113.8	113.3
7	95.5	106.7	81.0	106.1	110.1	112.1	110.5
8	97.8	100.5	71.4	99.3	105.0	108.1	108.5
9	92.3	96.9	74.8	98.3	105.7	105.5	104.6
10	89.2	94.2	67.5	96.8	102.2	101.9	100.7
11	95.0	91.8	71.7	96.1	96.2	100.0	100.9
12	82.6	90.2	67.1	91.7	98.3	98.2	98.3
13	83.5	88.0	75.1	90.8	95.7	97.8	95.2
14	80.8	87.9	75.6	90.5	92.3	95.0	90.9
15	79.8	89.6	69.2	92.1	91.4	95.1	92.9
16	78.2	84.1	69.0	89.5	91.6	94.1	92.2
17	79.3	84.1	73.7	86.3	89.1	92.8	90.4
18	80.6	82.8	68.0	87.6	89.2	93.7	91.1
19	77.8	83.5	67.9	87.5	89.4	92.9	91.1
20	**	85.7	71.5	86.8	90.0	93.0	90.9
Overall	123.4	128.1	100.6	128.1	131.9	133.9	133.6

*See Appendix A for frequencies

Table B-8. Interior Acoustic Pressure at Propeller
Blade Passage Frequencies - Location M11

Engine rpm	1700	2100			2400	2600	
Run Number	15	9	13	14b	11	12	12b
Operating Engines	Stbd	Both	Port	Stbd	Both	Both	Both
Harmonic Order*	Acoustic Pressure in dB (ref: 20μN/m²)						
1	92.7	100.7	99.9	93.7	104.1	104.4	104.7
2	86.3	97.0	86.6	96.2	98.9	100.1	100.2
3	87.7	88.4	77.7	86.7	92.7	91.5	90.6
4	78.9	80.7	76.3	77.2	90.3	88.4	87.8
5	75.3	80.2	75.6	86.3	82.4	93.1	94.8
6	83.9	82.3	71.0	86.3	87.2	87.9	88.5
7	73.2	84.9	75.1	85.3	82.8	87.5	87.1
8	77.3	71.5	62.0	76.2	81.9	81.8	77.9
9	71.1	74.9	61.2	76.8	75.4	78.0	78.1
10	65.2	70.4	64.3	68.6	72.3	77.7	72.9
11	66.4	68.5	64.0	72.4	73.3	76.5	70.9
12	62.6	63.9	64.1	68.6	71.9	73.3	69.7
13	58.6	69.7	63.7	68.3	66.7	72.3	66.8
14	57.3	65.5	61.9	64.6	65.7	71.3	68.2
15	55.9	60.1	56.3	57.4	63.3	70.8	67.9
16	58.0	59.0	55.2	58.8	64.3	71.4	69.8
17	54.3	61.1	52.8	56.6	67.3	**	63.5
18	52.3	56.5	53.0	53.6	61.6	**	63.2
19	49.8	57.3	**	55.3	61.1	**	62.9
20	49.0	56.6	**	57.7	62.1	**	**
Overall	95.2	102.6	100.2	99.2	105.7	106.4	106.6

* See Appendix A for frequencies
** No clearly defined spectral peak

Table B-9. Interior Acoustic Pressure at Propeller
Blade Passage Frequencies - Location M12

Engine rpm	1700	2100			2400	2600	
Run Number	15	9	13	14b	11	12	12b
Operating Engines	Stbd	Both	Port	Stbd	Both	Both	Both
Harmonic Order *	Acoustic Pressure in dB (ref: 20μN/m²)						
1	101.1	106.7	100.6	106.6	104.7	101.4	102.5
2	80.7	94.3	91.8	92.3	97.8	103.5	103.1
3	88.4	92.7	86.8	91.5	96.2	94.0	93.1
4	83.5	89.7	75.0	90.0	94.1	94.4	93.8
5	85.0	84.9	75.8	87.5	84.5	92.9	93.9
6	86.4	81.5	69.4	84.3	89.5	89.7	90.0
7	74.1	84.0	70.3	85.4	80.4	88.5	90.7
8	77.2	73.0	68.2	74.9	85.9	79.8	78.2
9	75.2	75.8	68.0	78.6	75.1	82.9	82.7
10	70.0	66.9	66.6	68.9	81.4	75.0	70.4
11	70.6	70.9	72.2	73.1	73.4	77.6	76.5
12	63.0	71.0	69.3	69.4	74.2	77.1	76.7
13	63.7	63.7	63.4	64.1	72.0	76.1	75.2
14	66.5	66.6	60.0	67.2	71.8	72.3	71.4
15	55.5	65.3	57.4	62.7	67.7	72.5	67.8
16	54.3	63.8	59.9	61.6	64.3	72.3	67.1
17	58.7	60.4	55.3	60.0	65.3	**	68.8
18	55.9	61.0	54.8	58.6	63.3	**	65.8
19	52.9	57.0	56.6	53.0	64.6	**	64.1
20	52.6	59.6	51.9	57.8	**	**	62.0
Overall	101.7	107.2	101.3	107.1	106.5	106.6	106.8

* See Appendix A for frequencies
** No clearly defined spectral peak

APPENDIX C

Vibration/Acoustic Frequency Response Functions
at Propeller/Blade Passage and Exhaust Frequencies

Table C-1. Magnitude of Frequency Response (Inertance) Function Between Microphone 4 and Accelerometer 1 For Various Test Runs

Engine rpm	1700	2100			2400	2600	
Run Number	15	9	13	14b	11	12	12b
Operating Engines	Stbd	Both	Port	Stbd	Both	Both	Both
Harmonic Order* Propeller / Exhaust	Inertance Magnitude in dB (ref: $1g/20\mu N/m^2$)						
1	**	-169.9	**	**	**	**	**
2	-168.5	**	-127.0	**	**	**	-154.8
3	-164.5	-147.7	-104.8	-138.6	-143.2	-148.2	-136.2
1 —	-140.1	-138.9	-122.8	-139.8	-141.0	-136.0	-136.4
4	**	**	**	**	**	**	**
5	-149.7	-146.9	-133.8	-139.2	-149.2	-156.4	-149.0
6	-135.7	-138.9	-131.8	-138.8	-136.6	-131.2	-130.6
7	-138.5	-142.9	-130.4	-132.4	-140.4	-132.0	-126.4
2 —	-122.9	-117.7	-115.6	-119.0	-113.2	-107.6	-109.2
8	-125.3	-124.7	-124.8	-125.4	-118.2	-126.6	-124.6
9	-130.5	-109.5	-108.0	-102.8	-125.6	-134.6	-134.6
10	-120.5	-126.1	-110.6	-119.6	-141.8	-142.6	-134.4
11	-115.5	-132.3	-125.8	-133.2	-135.2	-131.4	**
3 —	-103.7	-115.5	-120.2	-116.8	-118.2	-113.6	-116.2
12	-119.5	-131.7	-120.0	-130.8	-121.4	-119.8	-118.8
13	-131.9	-145.9	-114.4	-136.4	-126.0	-121.6	-122.0
14	-133.9	-123.9	-122.0	-122.8	-116.6	-119.0	-119.6
15	-136.9	-125.1	-131.4	-122.6	-120.0	-119.6	-119.4
4 —	-117.7	-111.5	-116.2	-111.6	-113.6	-113.4	-113.6
16	-130.7	-117.3	-116.6	-118.0	-118.2	-122.0	-120.0
17	-121.5	-124.1	-117.6	-123.6	-118.2	-118.8	-118.4
18	-120.7	-122.3	-120.6	-124.6	-121.8	-120.2	-118.4
19	-114.7	-119.1	-116.6	-116.4	-121.0	-117.2	-116.8
5 —	-112.3	-114.7	-117.6	-114.4	-113.6	-116.6	-117.4

* See Appendix A for frequencies
**No spectral peak or inadequate coherence

Table C-1. Magnitude of Frequency Response (Inertance)
Function Between Microphone 4 and Accelerometer 1
For Various Test Runs (Continued).

Engine rpm		1700	2100			2400	2600	
Run Number		15	9	13	14b	11	12	12b
Operating Engines		Stbd	Both	Port	Stbd	Both	Both	Both
Harmonic Order*		Inertance Magnitude in dB (ref: $1g/20\mu N/m^2$)						
Propeller	Exhaust							
	20	-123.1	-119.3	-118.2	-119.8	-119.2	-116.8	-116.4
	21	-120.1	-115.9	-117.0	-116.8	-114.8	-115.0	-115.4
	22	-122.5	-119.3	-117.2	-121.4	-120.2	-115.8	-116.0
	23	**	**	-119.2	**	**	**	-120.2
6	-	-116.3	-112.9	-115.4	-116.0	-120.0	-119.8	-121.2
	24	-122.5	-117.9	-118.4	-117.2	-115.4	-117.4	-117.0
	25	-126.7	-116.1	-122.4	-116.8	-117.4	-122.2	-120.8
	26	-122.5	-117.3	-109.8	-117.4	-118.0	-128.6	-123.2
7	-	-115.3	-115.7	-114.4	-124.4	-118.8	-115.4	-113.8
	27	**	**	**	-125.6	-117.0	**	**
	28	-116.1	-115.3	-121.0	-115.4	-120.8	-129.0	-129.4
	29	-114.9	-117.7	-119.2	-117.0	-128.0	-128.6	-130.0
	30	-118.7	-119.8	-118.0	-119.0	-126.2	-131.0	-130.0
8	-	-119.7	-115.5	-119.2	-114.8	-115.2	-114.4	-114.0
	31	**	**	-132.0	-115.6	-115.0	-116.8	**
	32	-116.1	-122.7	-116.8	-120.0	-122.6	-126.0	-122.8
	33	-116.7	-125.5	-118.2	-125.0	-129.0	-122.8	-122.6
	34	-116.3	-131.3	-123.4	-132.4	-130.4	-121.4	-117.2
9	-	-114.5	-114.7	-118.6	-113.4	-118.4	-113.2	-117.6
	35	-113.9	-123.9	-114.4	-116.6	-120.8	-116.0	-119.8
	36	-118.5	-124.3	-125.8	-125.4	-122.8	-117.6	-117.2
	37	-121.1	-128.1	-127.4	-122.2	-122.4	-123.6	-120.8
	38	-151.1	-124.5	-119.0	-124.0	-122.6	-126.4	-126.4
10	-	-115.1	-113.5	-120.6	-117.4	-110.6	-115.4	-121.4

* See Appendix A for frequencies
** No spectral peak or inadequate coherence

Table C-2. Magnitude of Frequency Response (Inertance) Function Between Microphone 7 and Accelerometer 4 For Various Test Runs

Engine rpm		1700	2100			2400	2600	
Run Number		15	9	13	14b	11	12	12b
Operating Engines		Stbd	Both	Port	Stbd	Both	Both	Both
Harmonic Order*		Inertance Magnitude in dB (ref: 1g/20µN/m²)						
Propeller	Exhaust							
	1	**	**	**	**	**	**	**
	2	-155.3	**	-129.7	**	-147.3	-141.6	-136.0
	3	-136.6	-126.1	-109.5	-124.3	-129.9	-129.0	-126.8
1	-	-144.1	-141.3	-139.4	-143.8	-136.4	-131.2	-131.2
	4	-144.0	**	-126.9	**	**	**	**
	5	-139.0	-134.7	-131.2	-134.1	-133.9	-132.9	**
	6	-128.9	-130.5	-127.3	-131.4	**	-120.7	-121.4
	7	-126.6	**	-131.2	**	-120.9	-115.8	-115.6
2	-	-126.8	-114.8	-116.1	-114.9	-110.1	-110.4	-111.0
	8	-128.4	-115.9	-129.0	-113.8	-115.7	-118.7	-119.8
	9	-130.3	-126.0	-106.0	-126.7	-126.8	-140.7	-137.8
	10	-109.5	-126.0	-127.1	-123.1	-131.8	**	**
	11	-124.0	-134.5	-113.1	-137.8	-129.6	**	-123.8
3	-	-118.1	-114.6	-118.4	-117.4	-111.3	-106.9	-108.4
	12	-118.3	-136.9	-115.1	-135.8	-124.0	-126.9	-122.8
	13	-130.8	-133.0	-126.6	-136.3	-129.4	-130.6	-128.4
	14	-125.2	-126.1	-125.4	-120.8	-124.9	-124.2	-125.0
	15	-129.6	-118.9	-115.5	-119.4	-125.1	-121.5	-121.6
4	-	-109.8	-115.0	-133.5	-115.9	-124.3	-114.8	-113.8
	16	-131.9	-123.1	-121.7	-125.7	-123.3	-125.5	-125.0
	17	**	-133.8	-118.5	-131.0	-112.3	-117.7	-119.0
	18	-124.6	-125.3	-113.1	-124.0	-126.4	-115.4	-114.6
	19	-116.8	-119.5	**	-124.5	-130.2	-127.3	-126.0
5	-	**	-117.4	-118.0	-121.1	-131.0	-116.8	-118.2

* See Appendix A for frequencies
**No spectral peak or inadequate coherence

Table C-2. Magnitude of Frequency Response (Inertance) Function Between Microphone 7 and Accelerometer 4 For Various Test Runs (Continued)

Engine rpm		1700	2100			2400	2600	
Run Number		15	9	13	14b	11	12	12b
Operating Engines		Stbd	Both	Port	Stbd	Both	Both	Both
Harmonic Order*		Inertance Magnitude in dB (ref: 1g/20µN/m²)						
Propeller	Exhaust							
	20	-143.4	-127.2	**	-129.7	-125.7	-125.1	-125.0
	21	-124.9	-117.4	-104.3	-117.2	-119.5	-125.6	-125.6
	22	-126.6	-122.8	-107.4	-122.6	-123.1	-132.2	-131.4
	23	**	**	-110.6	**	-125.4	**	**
6	-	-128.9	-122.8	**	-130.4	-122.8	-119.5	-115.0
	24	-129.8	-124.2	-118.0	-125.1	-128.1	-114.5	-115.6
	25	-131.0	-116.7	-120.8	-119.6	**	-124.6	-124.0
	26	-116.5	-125.4	-111.1	-124.4	-127.3	-132.0	-132.0
7	-	**	-124.8	-117.0	-123.7	**	**	-120.0
	27	**	**	**	**	-132.0	-122.6	-118.0
	28	-135.0	-123.1	-112.1	-125.8	-125.6	-126.2	-126.8
	29	-125.8	-119.2	-114.1	-124.0	-113.9	-123.3	-121.8
	30	-125.9	-125.9	-116.2	-128.9	-123.5	-125.2	-124.0
8	-	**	-128.5	-122.6	-128.6	-127.5	-126.5	-133.6
	31	-132.9	-123.5	**	**	-127.5	**	-129.2
	32	-122.8	-114.6	-122.9	-116.6	-134.0	-122.3	-119.8
	33	-125.5	-114.7	-119.2	-115.6	**	-122.0	-121.8
	34	-123.7	-119.8	-120.0	-120.7	**	-124.6	-124.8
9	-	-127.1	**	**	-134.0	-126.4	-122.9	-136.2
	35	-130.6	-129.8	-114.8	-128.0	-122.7	-125.2	-126.0
	36	-126.5	-122.5	-117.4	-123.1	-125.6	-130.6	-126.6
	37	-125.1	-126.5	-126.8	**	-127.3	-121.5	-119.4
	38	-127.5	-125.7	-122.0	-126.1	**	-121.2	-120.8
10	-	-131.3	-127.3	-125.1	**	-118.1	-119.8	-116.8

* See Appendix A for frequencies
** No spectral peak or inadequate coherence

Table C-3. Magnitude of Frequency Response (Inertance) Function For Various Transducer Pairs During Operation of Both Engines at 2600 rpm (Run 12b)

Harmonic Order*		Inertance Magnitude in dB (ref: 1g/20µN/m^2)				
Propeller	Exhaust	A2/M4	A3/M5	A3/M7	A5/M4	A5/M7
	1	**	**	**	**	**
	2	-158.6	-131.4	-145.7	**	-130.3
	3	-134.4	-127.4	-129.9	-129.3	-118.7
1	-	-139.2	-135.0	-135.5	-120.1	-117.3
	4	**	**	**	**	**
	5	-145.0	-132.4	-157.3	-134.3	-136.1
	6	-138.8	-132.0	-132.9	-131.7	-125.1
	7	-136.6	-124.8	-134.3	-131.7	-130.1
2	-	-134.8	-139.0	-139.1	-117.7	-110.5
	8	-133.0	-132.2	-132.1	-136.3	-135.1
	9	-125.8	-128.0	-133.3	-123.1	-128.1
	10	-137.6	-125.4	-130.9	-136.3	-123.1
	11	-130.4	-131.4	-134.1	-122.7	-131.3
3	-	-144.0	-123.8	-122.1	-124.3	-116.9
	12	-130.0	-126.6	-130.7	-130.1	-133.1
	13	-131.0	-127.2	-127.3	-125.1	-124.1
	14	-132.6	-127.8	-131.1	-121.7	-120.5
	15	-142.6	-126.4	-124.3	-128.1	-121.5
4	-	-139.8	-132.2	-124.3	-130.5	-117.5
	16	-133.0	-124.6	-122.5	-133.5	-131.7
	17	-138.4	-135.2	-134.7	-125.7	-122.5
	18	-133.2	-127.6	-122.5	-137.7	-137.3
	19	-144.6	-126.4	-135.3	-136.3	-127.5
5	-	-140.2	-122.0	-120.3	-124.9	-115.7

* See Appendix A for frequencies
** No spectral peak or inadequate coherence

Table C-3. Magnitude of Frequency Response (Inertance)
Function For Various Transducer Pairs During
Operation of Both Engines at 2600 rpm (Run 12b) (Cont'd)

Harmonic Order*		Inertance Magnitude in dB (ref: 1g/20μN/m²)				
Propeller	Exhaust	A2/M4	A3/M5	A3/M7	A5/M4	A5/M7
	20	-134.2	-133.2	-138.3	-133.5	-136.5
	21	-128.2	-122.8	-129.7	-127.1	-132.3
	22	-139.2	-128.6	-129.9	-136.9	-131.5
	23	**	**	**	**	**
6	-	-136.0	-127.6	-125.3	-133.1	-122.1
	24	-137.2	-120.6	-124.9	-128.5	-118.1
	25	-135.0	-122.4	-126.7	-135.1	-134.9
	26	-134.2	-139.6	-134.3	-129.5	-132.5
7	-	-137.8	-123.0	-121.5	-130.1	-123.7
	27	**	**	**	**	**
	28	-127.4	-119.6	-121.3	-130.7	-133.3
	29	-134.6	-130.6	-133.7	-118.5	-114.9
	30	-124.6	-124.6	-126.9	-115.1	-116.3
8	-	-139.6	-137.0	-134.5	-128.3	-119.9
	31	-138.0	-131.4	-137.5	-132.5	-122.1
	32	-137.2	-127.8	-127.3	-126.9	-124.7
	33	-139.0	-123.0	-128.7	-116.5	-116.9
	34	-136.0	-134.2	-132.5	-126.1	-136.5
9	-	-137.8	-125.8	-128.5	-125.9	-121.7
	35	-140.2	-128.8	-134.3	-130.1	-136.9
	36	-149.6	-130.8	-138.7	-127.7	-125.3
	37	-137.4	-124.8	-124.1	-123.3	-127.7
	38	-137.6	-128.4	-132.3	-127.1	-129.5
10	-	-147.0	-125.6	-123.5	-127.7	-119.9

* See Appendix A for frequencies
** No spectral peak or inadequate coherence
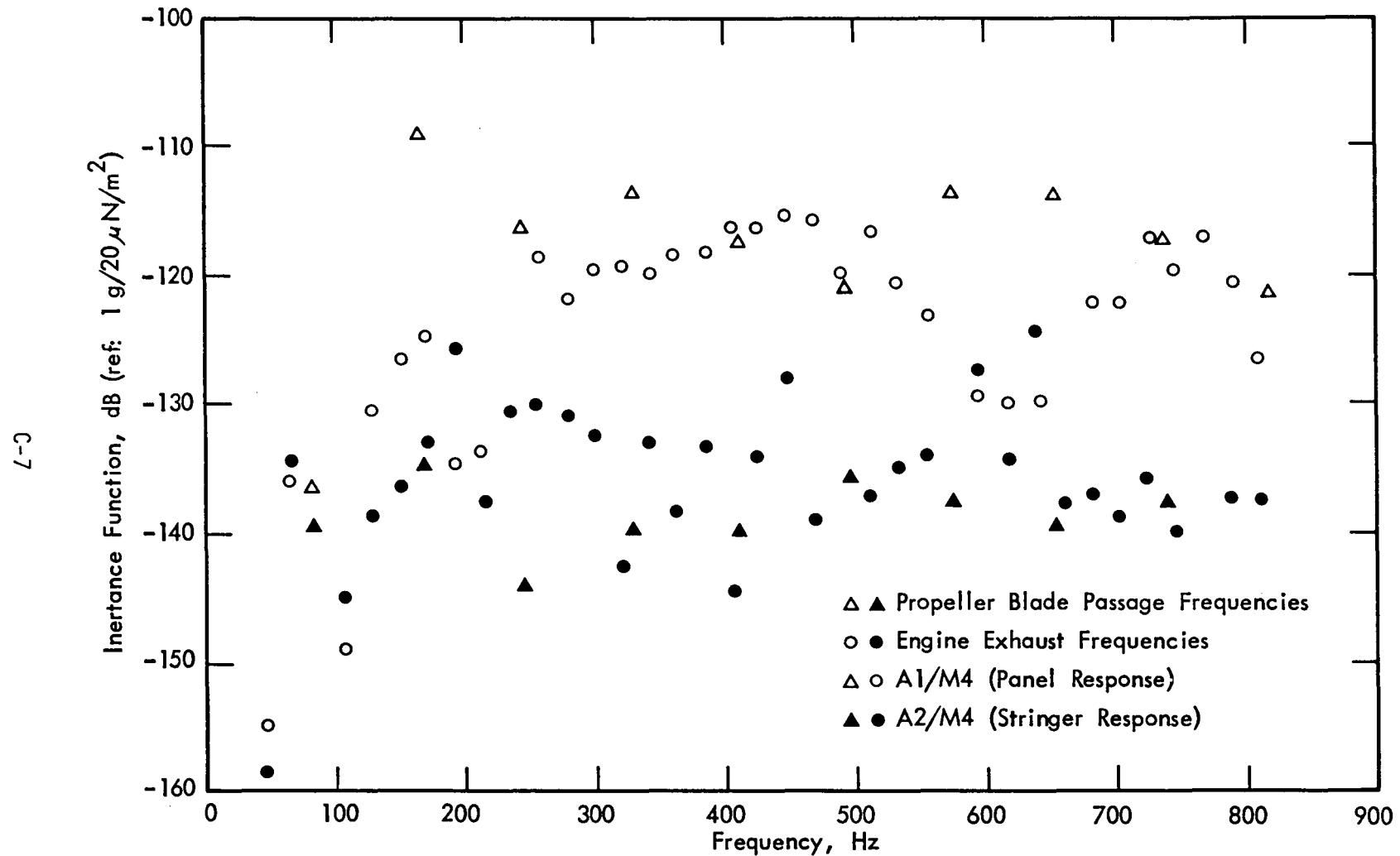
FIGURE C-1. MAGNITUDE OF FREQUENCY RESPONSE (INERTANCE) FUNCTIONS BETWEEN MICROPHONE 4 AND ACCELEROMETERS 1 AND 2 AT PROPELLER AND EXHAUST FREQUENCIES FOR OPERATION AT 2600 rpm (RUN 12b)
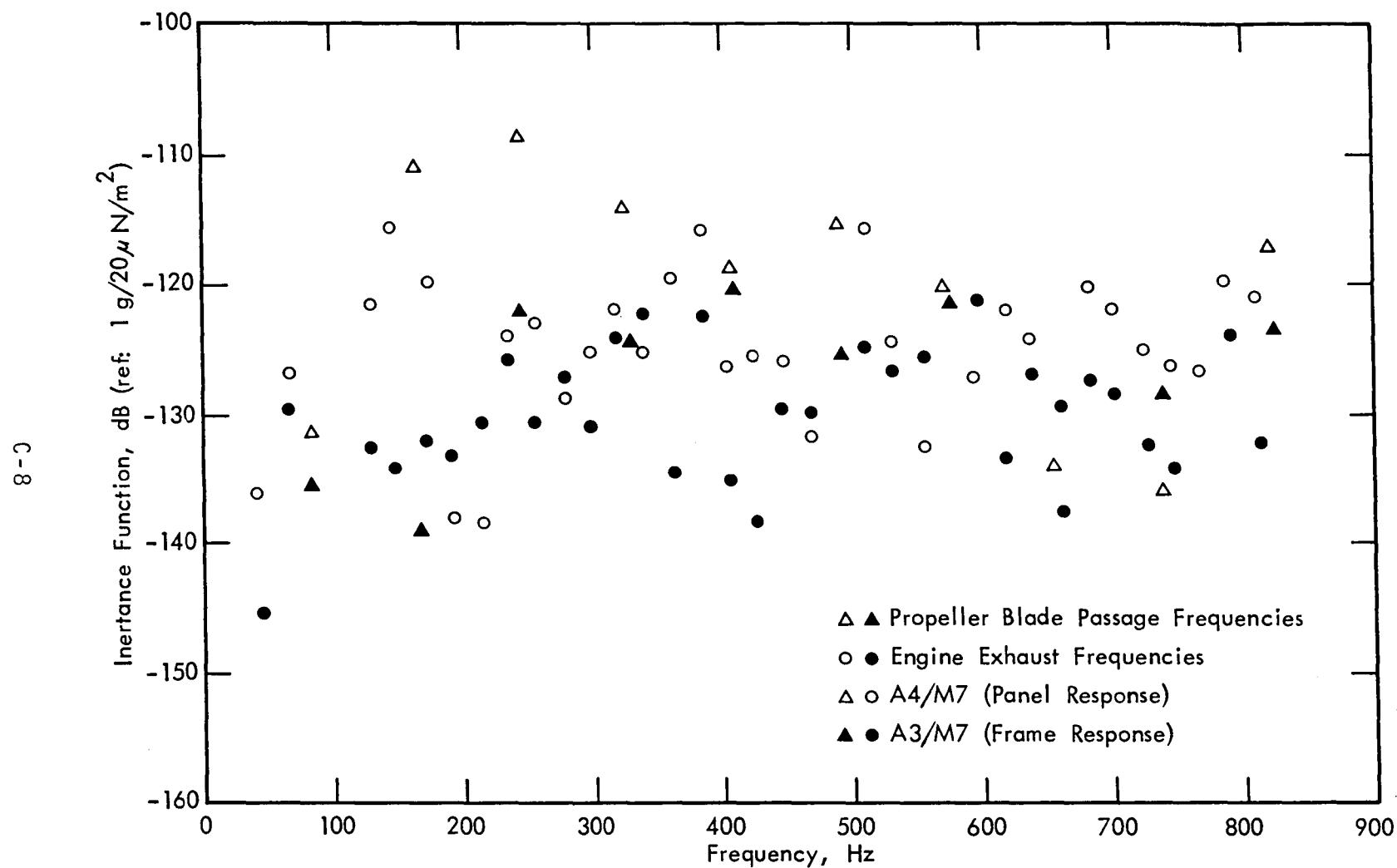
FIGURE C-2. MAGNITUDE OF FREQUENCY RESPONSE (INERTANCE) FUNCTIONS BETWEEN MICROPHONE 7 AND ACCELEROMETERS 3 AND 4 AT PROPELLER AND EXHAUST FREQUENCIES FOR OPERATION AT 2600 rpm (RUN 12b)
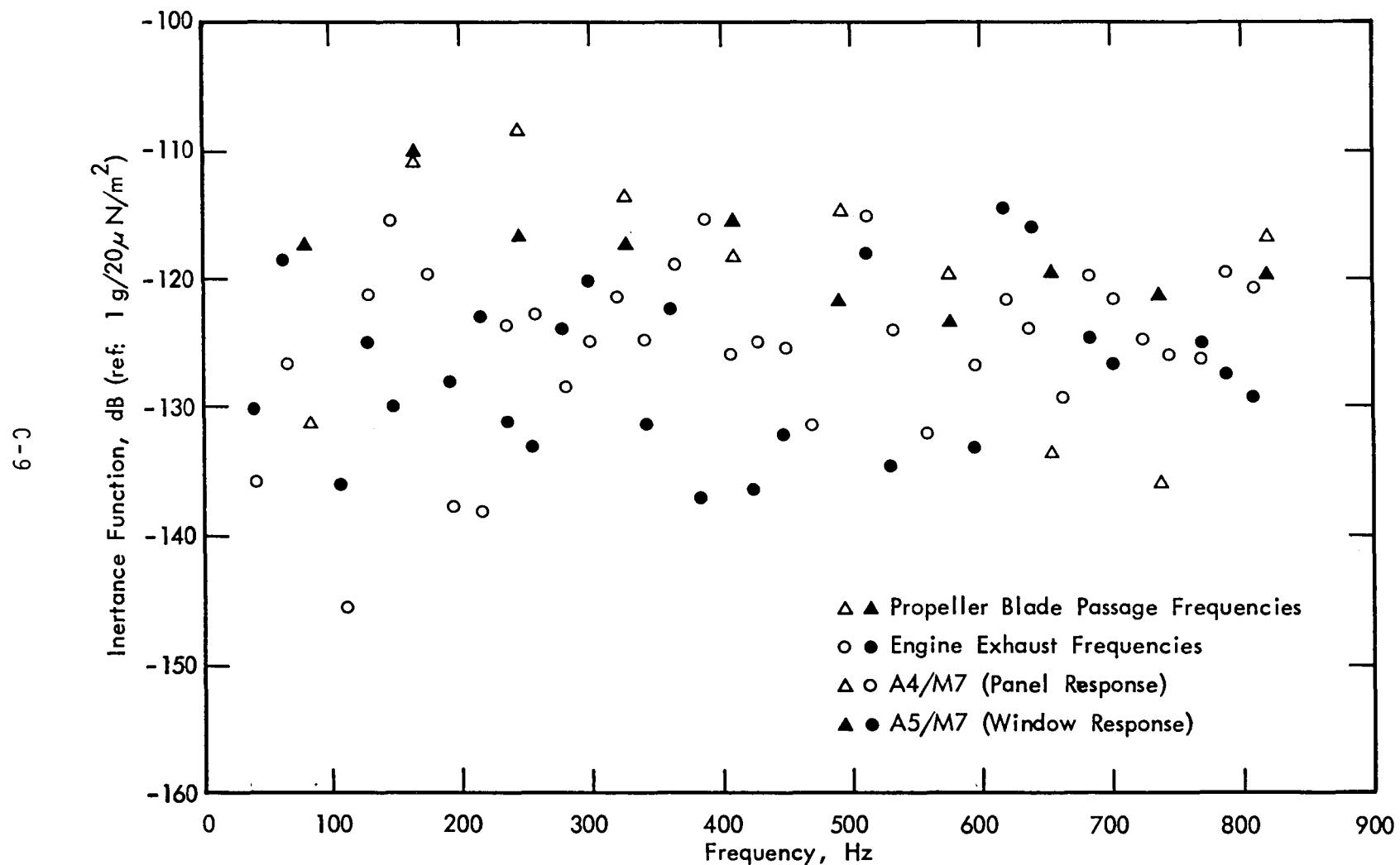
FIGURE C-3. MAGNITUDE OF FREQUENCY RESPONSE (INERTANCE) FUNCTIONS BETWEEN MICROPHONE 7 AND ACCELEROMETERS 4 AND 5 AT PROPELLER AND EXHAUST FREQUENCIES FOR OPERATION AT 2600 rpm (RUN 12b)

APPENDIX D

Phase Functions Between Spatially Separated Measurements
At Propeller Blade Passage and Exhaust Frequencies

Table D-1. Phase Functions Between Accelerometer 4 Versus 3 For Various Operating Conditions

Engine rpm		1700	2100	2400	2600
Run Number		15	9	11	12b
Operating Engines		Stbd	Both	Both	Both
Harmonic Order*		Phase Angle In Degrees			
Propeller	Exhaust				
	1	-11.8	1.1	**	**
	2	-17.4	3.4	- 4.3	1.3
	3	4.0	-5.0	- 1.4	-7.9
1	-	-6.5	10.6	29.4	17.5
	4	**	**	**	**
	5	-12.0	-16.2	- 3.9	-11.1
	6	-10.9	-7.9	-38.6	52.6
	7	-15.6	-12.9	-34.3	-34.6
2	-	-21.0	0.6	-19.6	-111.6
	8	-17.4	4.4	-82.5	-141.0
	9	16.7	-57.8	-153.2	-131.8
	10	-14.7	-111.4	-153.4	-6.5
	11	-119.3	158.3	-34.6	120.5
3	-	-35.4	52.4	-17.4	-54.5
	12	-95.4	-129.9	-135.2	179.8
	13	-177.4	-93.5	-127.2	121.9
	14	-104.7	-125.4	42.3	33.6
	15	-8.1	-114.7	70.4	72.8
4	-	14.0	-30.1	33.3	30.9
	16	-62.1	57.7	-12.4	-46.4
	17	-50.3	11.0	59.6	-1.0
	18	-179.6	15.7	80.0	-17.0
	19	-151.2	35.7	**	-2.8
5	-	-55.1	28.0	64.4	52.2

*   See Appendix A for frequencies
** No spectral peak or inadequate coherence

Table D-1. Phase Functions Between Accelerometer 4
Versus 3 For Various Operating Conditions
(Continued)

Engine rpm		1700	2100	2400	2600
Run Number		15	9	11	12b
Operating Engines		Stbd	Both	Both	Both
Harmonic Order*		Phase Angle In Degrees			
Propeller	Exhaust				
	20	11.3	-13.0	-32.1	-64.8
	21	71.8	-74.6	60.8	102.2
	22	52.4	-79.5	-101.4	154.4
	23	**	**	**	**
6	-	2.7	90.2	144.7	133.3
	24	-77.6	4.4	-1.0	-17.6
	25	-7.4	87.8	174.9	-10.9
	26	-35.8	-167.3	-34.0	-68.5
7	-	142.6	149.8	-12.6	99.8
	27	**	**	**	**
	28	-31.6	-17.0	-61.7	-96.1
	29	4.0	-161.5	-11.5	-111.0
	30	50.9	-44.9	-77.6	-98.1
8	-	153.2	15.1	-43.0	-151.0
	31	-177.9	-21.4	-177.6	-75.4
	32	-175.4	-23.1	-8.6	-21.0
	33	54.4	2.0	-95.8	-19.6
	34	7.3	-123.5	-52.6	-23.5
9	-	49.1	172.4	14.9	-31.2
	35	-117.6	-143.7	14.3	4.9
	36	19.4	-94.1	-28.1	-70.9
	37	-24.1	-24.3	-148.9	-6.5
	38	-46.0	-85.2	-29.3	0.2
10	-	-27.0	3.5	18.9	-25.7

 * See Appendix A for frequencies
 ** No spectral peak or inadequate coherence

Table D-2. Phase Functions Between Various Transducer Pairs During Operation of Both Engines at 2600 rpm (Run 12b)

Harmonic Order*		Phase Angle in Degrees By Transducer Pair					
Propeller	Exhaust	A1/A2	A1/A3	A1/A4	A1/A5	M5/M4	M5/M7
	1	**	**	-3.6	-0.7	-49.1	22.0
	2	1.8	7.2	3.5	3.0	56.2	63.7
	3	4.4	-6.3	1.3	-3.6	-13.2	-10.1
1	-	1.8	-1.2	-18.8	-158.9	35.0	93.0
	4	**	**	**	**	**	**
	5	42.3	39.2	38.0	-152.2	29.5	53.9
	6	17.3	168.3	111.7	81.3	-29.8	-7.6
	7	111.9	167.5	-161.6	-142.5	-42.1	-20.5
2	-	71.7	121.2	-124.2	-115.6	176.5	104.6
	8	62.0	1.8	-4.3	-86.6	6.4	-60.4
	9	40.6	21.9	162.7	-132.4	2.1	-21.1
	10	36.7	69.8	51.6	-77.8	-43.5	-58.3
	11	65.1	-176.5	129.3	-47.1	-61.0	-21.5
3	-	-61.9	114.2	168.6	108.9	120.6	116.0
	12	31.1	50.7	-122.0	131.4	74.0	-62.7
	13	39.0	73.3	-49.7	-179.8	-7.2	-71.9
	14	-49.3	-15.6	-49.4	168.6	35.2	-81.1
	15	-8.6	79.4	5.5	-133.8	-9.5	-110.2
4	-	173.1	43.6	12.7	15.4	164.4	-164.9
	16	-17.0	26.8	71.1	-166.2	10.1	-94.3
	17	-103.7	-11.4	-9.1	151.8	9.7	171.3
	18	158.1	58.1	72.7	-94.0	-23.8	-109.7
	19	-55.8	101.3	119.8	-20.3	-13.8	-136.0
5	-	-102.9	-87.6	-141.0	-5.3	-156.6	8.8

*   See Appendix A for frequencies
** No spectral peak or inadequate coherence

Table D-2. Phase Functions Between Various Transducer
Pairs During Operation of Both Engines at
2600 rpm (Run 12b) (Continued)

Harmonic Order*		Phase Angle in Degrees By Transducer Pair					
Propeller	Exhaust	A1/A2	A1/A3	A1/A4	A1/A5	M5/M4	M5/M7
	20	-47.4	40.6	103.5	16.0	-6.5	-122.3
	21	-70.9	-58.0	-161.4	-139.6	35.9	-120.0
	22	-25.0	46.3	-109.4	40.8	7.9	-88.9
	23	-110.6	-132.1	85.0	-33.9	-100.6	**
6		-123.8	-89.2	144.4	-95.8	-106.6	140.9
	24	-53.8	144.7	165.5	44.2	-47.1	-37.6
	25	-59.5	127.6	140.6	-30.4	-146.1	-125.4
	26	47.2	31.1	-108.6	19.6	106.2	63.3
7	-	-113.0	-66.5	147.4	-50.0	-89.3	143.3
	27	**	**	**	**	**	**
	28	-157.2	13.2	82.8	-18.3	9.4	-159.2
	29	83.4	-71.1	38.7	154.7	164.2	-131.1
	30	-171.6	101.3	-179.1	-71.2	-96.0	110.3
8	-	101.3	51.9	-134.1	64.3	-40.0	-73.7
	31	82.7	58.1	-141.2	47.9	-47.6	-24.2
	32	1.8	1.3	18.7	-11.3	-56.1	-23.2
	33	166.2	-140.0	-107.5	-143.8	15.6	152.6
	34	5.8	27.1	50.9	-126.0	14.8	158.8
9	-	59.8	158.7	45.5	148.6	3.9	78.9
	35	-122.9	64.4	33.6	-34.1	-23.2	-55.7
	36	-91.4	72.5	177.9	-146.4	-1.8	78.0
	37	-8.9	83.8	85.7	-163.3	-29.8	175.9
	38	66.6	146.3	176.5	23.9	-58.1	-59.5
10	-	19.2	-179.9	-151.3	64.8	36.1	-86.0

* See Appendix A for frequencies
** No spectral peak or inadequate coherence

APPENDIX E

Coherent Output Power Functions Between
Interior Microphones and Sidewall Vibration
At Propeller Blade Passage and Exhaust Frequencies

Table E-1. Differences Between Spectral Values and Coherent Output Power Values at Microphone 11 for Operation of Both Engines at 2600 rpm (Run 12b)

Har.* Order Eng. Prop	$G_{yy}(f)-G_{y:x}(f)$ in dB by Accelerometer No.					Har.* Order Eng. Prop	$G_{yy}(f)-G_{y:x}(f)$ in dB by Accelerometer No.				
	A1	A2	A3	A4	A5		A1	A2	A3	A4	A5
1	**	**	**	**	**	20	0.5	0.4	0.9	0.4	2.9
2	6.0	3.8	3.9	4.4	4.3	21	0.3	0.2	0.1	0.2	0.7
3	1.0	0.6	1.1	0.9	0.4	22	0.6	0.4	0.9	2.0	1.9
1	3.2	2.6	3.3	3.6	5.0	23	**	**	**	**	**
4	**	**	**	**	**	*6*	8.7	2.8	1.8	1.5	3.8
5	9.4	3.1	3.1	3.6	9.3	24	0.5	0.8	0.8	0.7	0.8
6	0.4	8.0	2.4	0.3	4.4	25	2.0	1.2	0.8	0.8	3.5
7	5.8	0.7	0.6	0.4	3.8	26	6.6	6.1	8.3	5.0	3.6
2	1.3	1.5	1.2	1.4	1.6	*7*	2.3	4.5	3.4	5.9	1.4
8	**	**	**	**	**	27	**	**	**	**	**
9	3.7	0.3	0.6	3.0	0.9	28	9.8	0.6	0.6	1.5	4.0
10	*	2.9	3.7	6.5	5.7	29	2.5	0.9	5.2	1.5	0.1
11	*	3.2	4.2	4.8	9.1	30	8.0	0.2	0.3	0.9	0.3
3	1.0	0.6	0.8	0.9	1.6	*8*	1.9	7.0	4.9	7.8	4.7
12	2.4	0	0	0	0	31	**	**	**	**	**
13	1.2	0.6	0.5	0.6	0.7	32	3.4	4.8	1.8	2.4	5.9
14	0.6	0.4	0.4	0.6	0.7	33	3.8	6.2	2.4	3.2	2.2
15	0.3	0.3	0.3	0.3	0.7	34	**	**	**	**	**
4	5.4	4.7	5.2	4.4	3.6	*9*	8.4	2.4	2.8	8.3	2.2
16	1.2	1.2	1.1	1.7	4.8	35	**	**	**	**	**
17	1.5	1.3	3.1	1.3	1.0	36	5.5	8.0	6.1	4.3	7.9
18	1.1	0.8	0.5	0.2	0.9	37	**	**	**	**	9.8
19	**	**	**	**	**	38	**	4.4	9.1	7.1	8.0
5	2.0	0.8	1.0	1.5	1.0	*10*	5.5	6.7	**	8.6	9.0

** No clearly defined spectral peak
* See Appendix A for frequencies

Propeller Harmonic Order*	$G_{yy}(f)-G_{y:x}(f)$ in dB by Run and Accelerometer No.									
	2100 rpm							2600 rpm		
	Run 9 (both)			Run 14b (Stbd)			Run 13 (port)	Run 126 (both)		
	A1	A4	A5	A1	A4	A5	A1	A1	A4	A5
At Microphone No. 11										
1	12.5	10.9	8.3	0.5	1.2	0.3	0.2	3.2	3.6	5.0
2	0.7	0.7	0.8	0.4	0.3	0.3	1.0	1.3	1.4	1.6
3	0.9	1.0	0.9	0.9	0.9	0.9	5.4	1.0	0.9	1.6
4	12.9	10.3	9.4	2.1	2.7	1.7	3.4	5.4	4.4	3.6
5	8.4	3.7	1.3	1.3	1.4	0.1	2.1	2.0	1.5	1.0
6	3.1	6.6	1.2	5.1	3.8	0.5	11.5	8.7	1.5	3.8
7	12.8	5.4	9.9	7.7	5.5	5.4	1.8	2.3	5.9	1.4
8	14.4	6.8	3.7	2.9	2.6	2.8	10.0	1.9	7.8	4.7
9	10.2	5.7	1.9	1.9	15.1	1.6	11.0	8.4	8.3	2.2
10	1.5	3.1	2.3	11.9	5.1	11.7	3.7	5.5	8.6	9.0
At Microphone No. 12										
1	0.8	0.9	0.7	0.1	0.6	0.2	0.1	1.4	1.9	2.7
2	2.0	2.1	2.1	0.4	0.5	0.6	1.0	0.6	0.4	0.4
3	0.3	0.7	0.5	0.4	0.8	0.6	3.4	1.0	0.4	0.3
4	2.7	4.8	3.1	1.4	2.3	1.8	2.7	1.1	0.8	1.0
5	3.2	0.3	0.8	1.8	0.3	0.5	3.9	1.0	0.8	0.2
6	1.7	2.1	2.5	4.5	4.7	1.0	8.4	6.0	1.9	1.4
7	5.9	2.6	9.3	5.2	2.3	3.1	2.7	2.0	5.4	1.3
8	10.4	13.7	3.9	3.0	2.2	1.8	4.4	1.5	7.8	1.6
9	16.9	5.8	1.1	3.5	13.5	1.5	12.1	9.8	12.5	0.6
10	**	**	**	**	**	**	4.5	**	**	**

* See Appendix A for frequencies
** No clearly defined spectral peak

APPENDIX F

Interior Sound Levels

Introduction

A fairly detailed analysis of the propeller-induced noise levels measured at microphone location M11 during earlier tests on the Aero Commander Airplane is contained in Appendix E of [2]. The purpose of this appendix is to provide a brief documentation of the interior noise levels measured during the present tests, the discussion being restricted to a comparison of average harmonic levels and beat characteristics with those of preceding tests. A detailed listing of harmonic levels measured at microphone locations M11 and M12 is given in Appendix B.

Average Harmonic Levels

It was observed in [2] that average harmonic levels, measured at microphone location M11 showed differences of up to 6 dB between the static-operation [1] and taxi-operation [2] test series (referred to as Test Series I and II, respectively). The differences were attributed to influences of the wind in Test Series II. The comparison of harmonic levels given in Table E-3 of [2] for an engine speed of 2600 rpm is now repeated here in Table F-1, with the addition of data from the present tests.

The data in Table F-1 show good agreement between the present test results and those from Test Series 1, with the average difference in harmonic level being about 0.9 dB and the maximum difference 2.4 dB. Agreement is poor between present results and Test Series 2 data (average difference 2.9 dB and maximum difference 6.3 dB). This comparison lends support to the explanation given in [2] that static test results from Test Series 2 are influenced by ambient wind conditions.

Table F-1. Average Propeller Harmonic Sound Levels For
Interior Microphone Location #11: Static
Condition, 2600 rpm (2 Hz Resolution)

Harmonic Number	Average Harmonic Sound Level (dB)		
	Test Series I	Test Series II	Present Tests
1	105.6	105.2	104.6
2	100.2	101.7	100.2
3	92.9	94.0	91.1
4*	87.4	88.8	88.1
5	93.9	88.7	94.0
6	88.7	84.0	88.2
7*	88.3	82.2	87.3
8	81.1	75.3	79.9
9	76.4	71.8	78.1
10*	74.2	70.1	75.3
11*	74.5	72.6	73.7
12	71.9	70.5	71.5
13	68.9	70.2	69.6
14*	67.4	68.7	69.8
15	69.4	65.8	69.4

*These data points are contaminated by exhaust noise.
 Contamination may also occur at other harmonics, particularly
 those of higher order.

Beat Characteristics

Discussion of the beat characteristics associated with the sound
levels at microphone location M11 is given in Appendix E of [2]
where it is shown that the beat amplitude can be interpreted in
terms of the different contributions from left and right hand
propellers, although the method cannot identify the propeller
making the greater contribution to the sound level. Furthermore,
it was shown that the time-averaged sound level is a meaningful
measure even in the presence of a beat with a large amplitude.

The beat characteristics observed in the present test data are
similar to those from previous tests. For example, the time
histories plotted in Figure F.1 for the propeller blade passage
frequency are typical of those presented in [2] in terms of
beat frequency and peak-to-peak amplitude. Pertinent parameters
for the present test data are given in Table F-2. For all tests,
the maximum beat frequency is 2.24 Hz, which is similar to the
corresponding value of 2.65 Hz in Table E-6 of [2]. This fre-
quency denotes the maximum difference between blade passage
frequencies for the two propellers.

The propeller harmonic sound levels at a given point in the fuse-
lage result from contributions from the two propellers. It is
unlikely that the two contributions will be equal in level and
it has been shown in Appendix E of [2] that the beat amplitude
can be used to estimate the difference in level between the con-
tributions from the two propellers. The smaller the beat ampli-
tude, the greater is the difference between the contributions
from the different propellers. Table F-2 shows the beat ampli-
tude for the first and second propeller harmonics for the two
measurement locations and several test conditions. The beat

amplitudes are then translated into the difference between the contributions from the two propellers, using Figure E-8 of [2]. Also Table F-2 shows the difference in level between each propeller contribution and the measured combined harmonic level. (The analysis cannot determine which propeller generates the higher sound level at a given measurement location).

Results in Table F-2 show that, although in several cases the difference in contributions from the two propellers is only 2 or 3 dB for a given harmonic and location, there are cases where one propeller generates levels which are 5.5 to 8.5 dB higher than the levels associated with the other propeller. Under these circumstances one propeller dominates the harmonic sound level at the measurement location. This is evident in Table F-2. These results are consistent with those presented in [2] from earlier tests on the Aero Commander test airplane.
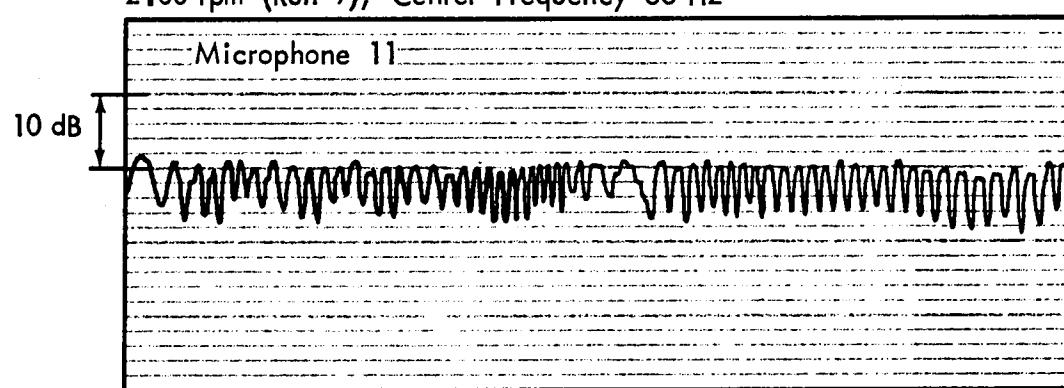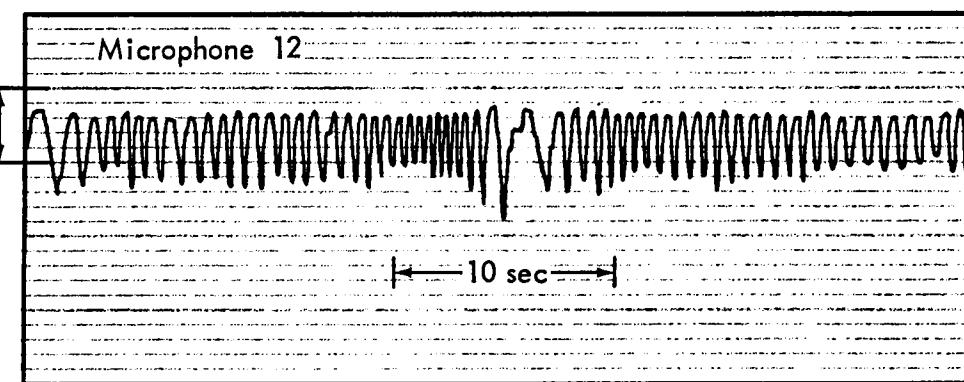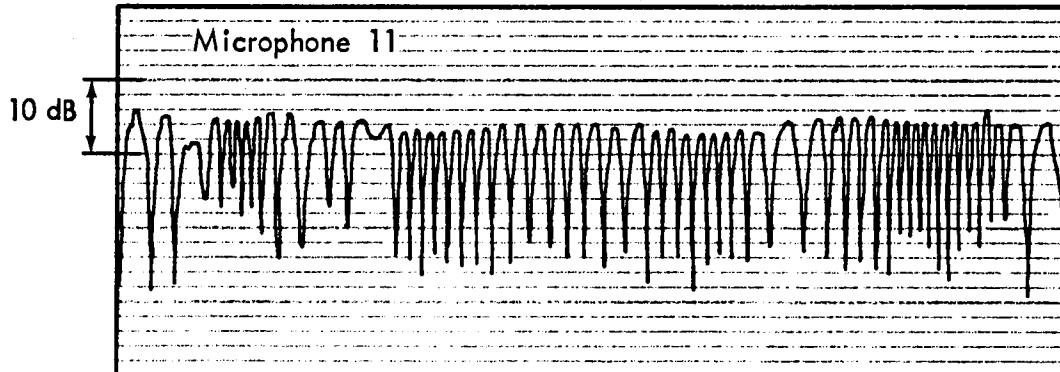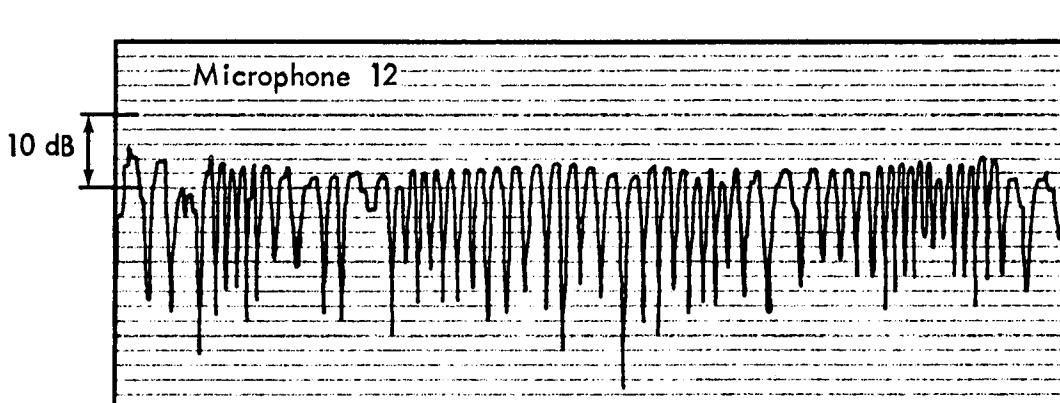
FIGURE F-1. CABIN NOISE TIME HISTORIES FOR PROPELLER BLADE PASSAGE FREQUENCY (FIRST HARMONIC)

Table F-2. Properties of Acoustic Beats at Microphone Locations M11 and M12

Run	RPM	Microphone	Harmonic Order	Max. Beat Frequency (Hz)	Typical Beat Peak-to-Peak Amplitude (dB)	$SPL_{max}-SPL_{min}$ (dB)	Total-SPL_{max} (dB)	Total-SPL_{min} (dB)
9	2100	M11	1	2.24	7	8.5	0.6	9.1
			2		7.5	7.5	0.7	8.2
		M12	1		10	5.5	1.1	6.6
			2		15	3	1.8	4.8
11	2400	M11	1	2.22	19	2	2.1	4.1
			2		9	6.5	0.9	7.4
		M12	1		15	3	1.8	4.8
			2		18	2	2.1	4.1
12	2600	M11	1	0.75	16	3	1.8	4.8
			2		10	5.5	1.1	6.6
		M12	1		19	2	2.1	4.1
			2		12	4.5	1.3	5.8
12b	2600	M11	1	2.20	18	2	2.1	4.1
			2		16	3	1.8	4.8
		M12	1		20	2	2.1	4.1
			2		9	6.5	0.9	7.4

1. Report No. NASA CR-159290	2. Government Accession No.	3. Recipient's Catalog No.
4. Title and Subtitle EVALUATION OF AERO COMMANDER SIDEWALL VIBRATION AND INTERIOR ACOUSTIC DATA: STATIC OPERATIONS		5. Report Date October 1980
		6. Performing Organization Code
7. Author(s) A.G.Piersol, E. G. Wilby, J. F. Wilby		8. Performing Organization Report No. 4016
		10. Work Unit No.
9. Performing Organization Name and Address Bolt Beranek and Newman Inc. 21120 Vanowen Street Canoga Park, CA 91303		11. Contract or Grant No. NAS1-14611-32
		13. Type of Report and Period Covered Contractor Report
12. Sponsoring Agency Name and Address National Aeronautics and Space Administration Langley Research Center Hampton, Virginia 23665		14. Sponsoring Agency Code

15. Supplementary Notes

Contract Monitor: Dr. John S. Mixson, NASA Langley Research Center

16. Abstract

Aero Commander vibration and acoustic test data have been analyzed to determine

(a) vibration and pressure levels, due to propeller excitation, at various locations on the fuselage and in the cabin,

(b) frequency response (inertance) functions between exterior pressures and fuselage vibration for propeller and engine exhaust noise,

(c) relative phase between spatially-separated vibration responses,

(d) coherent output power functions at interior microphone locations based upon individual sidewall vibration responses.

On the basis of the five accelerometer locations, the fuselage skin panels near the plane of rotation of the propeller appear to accept propeller noise excitation more efficiently than they do exhaust noise. Coherent output power measurements could distinguish between contributions from left and right hand propellers, as they occurred at different frequencies, but they could not identify the relative roles played by different structural regions in transmitting sound. Comparisons between predicted and measured inertance functions show only moderate agreement.

17. Key Words (Suggested by Author(s)) Propeller noise Engine exhaust noise Fuselage vibration Airplane interior noise	18. Distribution Statement

19. Security Classif. (of this report) Unclassified	20. Security Classif. (of this page) Unclassified	21. No. of Pages 86	22. Price*

End of Document